THE ASTROPHYSICAL JOURNAL, 321:251–279, 1987 October 1

A DETAILED STUDY OF THE C IV λ1550 LINE PROFILE AND ADJACENT SPECTRAL FEATURES IN NGC 4151 FROM 1978 TO 1983[1]

J. CLAVEL,[2,3] A. ALTAMORE,[4] A. BOKSENBERG,[5] G. E. BROMAGE,[6] A. ELVIUS,[7] D. PELAT,[8] M. V. PENSTON,[5] G. C. PEROLA,[4] M. A. J. SNIJDERS,[5] AND M. H. ULRICH[9]

Received 1986 August 11; accepted 1987 March 16

ABSTRACT

The 1450–1720 Å spectral region of NGC 4151 is analyzed by means of Gaussian decomposition for 69 different epochs, from early 1978 to the end of 1983.

The C IV λ1550 emission profile is well represented by a core, whose full width at half-maximum (FWHM) varies between 2600 and 5500 km s^{-1}, and an ultrabroad component (14,600 km s^{-1} FWHM). The variations of intensity of the broad feature follow closely those of the continuum, with a delay that implies that the broad feature originates in a region whose "radius" is ~5 lt-day. The gas density definitely exceeds 7×10^{10} cm^{-3} and probably reaches 10^{11} cm^{-3} in this innermost region. A dimension of ~25 lt-day is found for the lower velocity region where the C IV core is emitted. A broad (8600 km s^{-1} FWHM) He II λ1640 component which originates in a region whose radius is ~15 lt-day is also detected. A fourth subregion is identified which emits the N IV] λ1485, the O III] λ1663, the core of He II λ1640 as well as the core of the C III] λ1908 line, and the "broad" [O III] λ5007 feature detected in the optical. By its dimension (250 lt-day), velocity dispersion (1600 km s^{-1}), and density (10^7 cm^{-3}), it represents a transition between the narrow- and broad-line regions in NGC 4151.

The radius and the inverse square root of the velocity dispersion are linearly correlated. This indicates that the motion of the gas is Keplerian and yields a value of $(3.7 \pm 0.5) \times 10^7\ M_\odot$ for the central mass.

In a previous paper, we proposed that the unidentified L1 λ1518 and L2 λ1594 emission features are Doppler-shifted C IV λ1550 lines excited by the two-sided radio jet impinging on the broad-line clouds. The present study confirms that their intensities are *not* correlated with the continuum flux, but are well correlated one with the other, especially on short time scales, a fact which strengthens our hypothesis. Moreover, if present any time delay between the variations of L1 and L2 has to be smaller than 4 days. This constrains the jet to be almost in the plane of the sky and puts the obstacles in the region where the ultrabroad C IV line is formed.

A correlation is found between the wavelength of the ultrabroad C IV λ1550 component and its intensity. It strongly suggests the existence of a *decelerated outflow* whose velocity is ~4000 km s^{-1} at 5 lt-day from the nucleus. However, this requires that the inner part of the wind is partially obscured. We propose that an accretion disk, seen almost edge-on, provides both the obscuration mechanism and the material to replenish the continuously forming wind.

Subject headings: galaxies: individual (NGC 4151) — galaxies: Seyfert — ultraviolet: spectra

I. INTRODUCTION

NGC 4151 is a prominent Seyfert class I galaxy (Khachikian and Weedman 1974). In other words, its permitted emission lines are substantially broadened (by at least 4000 km s^{-1}), so that it may be termed a "miniquasar." As a consequence, the nucleus of this nearby ($z = 0.0033$) galaxy has been much studied at all wavelengths.

The authors have contributed to this effort by amassing a substantial data base of ultraviolet spectra of NGC 4151 taken from the *International Ultraviolet Explorer* (*IUE*) satellite. Results from this monitoring program have been published in a series of papers (Penston *et al.* 1981; Perola *et al.* 1982; Ulrich *et al.* 1984; Bromage *et al.* 1985; Ulrich *et al.* 1985; Perola *et al.* 1986; hereafter papers I–VI, respectively), and the data will soon be presented as an atlas (Snijders *et al.* 1987). These data cover the variations in the ultraviolet spectrum of the galaxy from 1978 until the time of writing (late 1985). The variations are complex and appear to contain evidence crucial to a full understanding of the central regions of NGC 4151. Certainly, the relationship of the variations of different spectral components is the only way we have of studying the spatial structure of the Seyfert nucleus on a length scale of $\sim 10^{16}$ cm (~30 micro-arcsec at the distance of NGC 4151 taken to be 20 Mpc throughout this paper).

In Paper III, we have shown that the emission lines vary in response to changes in the continuum but with lags that differed from line to line. These lags appeared to be correlated with the line width, and this led us to propose that the broad-line region (BLR) in NGC 4151 was stratified. We characterized the stratification by dividing the BLR into three subregions of different excitation, internal velocity dispersion, and distance from the continuum source. However, we were very conscious that the choice of the number of subregions was

[1] Based on observations made with the *IUE* and collected at the Villafranca satellite tracking station (ESA).

[2] Affiliated with the Astrophysics Division, Space Sciences Department, ESTEC, The Netherlands.
[3] ESA-*IUE* Observatory, Madrid.
[4] Istituto Astronomico, Rome.
[5] Royal Greenwich Observatory, UK.
[6] Rutherford and Appleton Laboratory, UK.
[7] Stockholm Observatory, Sweden.
[8] Observatoire de Meudon, France.
[9] European Southern Observatory, FRG.

driven by the fact the *IUE* data cover three strong emission lines.

Some of the emission features are blended with the absorption lines which are discussed in Paper IV and subsequently by Veron, Veron-Cetty, and Tarenghi (1985), who introduced a controversial element by advocating a very different interpretation of their variations than that presented in Paper IV. Crude methods may yield considerable uncertainties in the absorption equivalent widths because of difficulties in constructing local continua. An additional blending problem is introduced by the sharp, variable, and so far unidentified emission lines, L11 λ1518 and L2 λ1594, which may well be Doppler-shifted satellites of C IV λ1550 associated with an SS 433–like jet in the nucleus of NGC 4151 (Paper V).

Overall, blending is a very serious problem in the ultraviolet spectrum of NGC 4151, most notably in the region around the C IV λ1550 doublet where many important spectral features occur.

In order to clarify these matters, and originally motivated by the wish to make more precise the division of the broad-line region into subregions (BLR1, BLR2, and BLR3), we embarked on an attempt at line-profile fitting of the C IV region for all spectra from our data base between 1978 and 1983. This paper reports the difficulties and achievements of this study.

II. THE DATA AND THEIR ANALYSIS

a) Choice of a Model Decomposition

The different spectral components which enter our decomposition of the 1450–1720 Å spectral region are listed in Table 1. We shall spare the reader the long history of the various

TABLE 1

MODEL ADOPTED FOR THE C IV λ1550 LINE PROFILE DECOMPOSITION

Component ID	Parameter	Freedom	Value (if fixed) & units
	Io	Free	10^{-13} erg/cm^2/s/A
NIV]1485 Emission	Lo	Free	A
	FWHM	Fixed	1600 km/s
	Io	Free	10^{-13} erg/cm^2/s/A
L1 1518 Emission	Lo	Free	A
	FWHM	Fixed	1600 km/s
	To	Free	Optical depth
CIV 1548.2 Absorption	Lo	Free	A
	FWHM	Fixed	1300 km/s
	To	Fixed	0.7*To(1548.2)
CIV 1550.8 Absorption	Lo	Fixed	Lo(1548.2)*1550.8/1548.2
	FWHM	Fixed	1300 km/s
	Io	Free	10^{-13} erg/cm^2/s/A
CIV 1549.5 Emission	Lo	Free	A
CORE	FWHM	Free	km/s
	Io	Free	10^{-13} erg/cm^2/s/A
CIV 1549.5 Emission	Lo	Free	A
BROAD	FWHM	Fixed	14600 km/s
	Io	Free	10^{-13} erg/cm^2/s/A
L'2 1576 Emission	Lo	Free	A
	FWHM	Fixed	1600 km/s
	Io	Free	10^{-13} erg/cm^2/s/A
L2 1594 Emission	Lo	Free	A
	FWHM	Free	km/s
	Io	Free	10^{-13} erg/cm^2/s/A
HeII1640.5 Emission	Lo	Fixed	1640.5 A
CORE	FWHM	Fixed	1600 km/s
	Io	Free	10^{-13} erg/cm^2/s/A
HeII1640.5 Emission	Lo	Free	A
BROAD	FWHM	Fixed	8600 km/s
	Io	Free	10^{-13} erg/cm^2/s/A
OIII]1663 Emission	Lo	Free	A
	FWHM	Fixed	1600 km/s
Continuum at 1450 A	F(1450)	Free	10^{-13} erg/cm^2/s/A
Continuum at 1710 A	F(1710)	Free	10^{-13} erg/cm^2/s/A

trials which led to this particular model and stress instead only a few relevant points.

The 1430–1470 Å and 1700–1720 Å continuum "windows" are devoid of spectral lines (Paper I), so that the analysis can be conveniently restricted to the 1450–1720 Å interval.

The spectral region around the C IV λ1550 line is a blend of seven different emission features and one absorption feature which are all variable: N IV] λ1483.3/1486.5, L1 λ1518.3, C IV λ1548.2/1550.8 (emission and absorption), L'2 λ1578, L2 λ1594.3, He II λ1640.5, and O III] λ1660.8/1666.2 (see Paper I and, for the "satellite" L1, L2, and L'2 lines, see Paper V).

The C IV λ1550 and He II λ1640 emission lines have very broad wings (~30,000 and ~20,000 km s^{-1} full width at zero intensity, respectively) underlying a much narrower core (~4000 and ~1600 km s^{-1} FWHM, respectively). A single functional form, be it a Gaussian, a Lorentzian, or a triangle, is inadequate to fit such profiles. While a Voigt function might conceivably be able to reproduce this type of shape, we have preferred the use of two Gaussians, which has the advantage over the Voigt function that it can take into account the existence of asymmetries in the profile. The number of free parameters turns out to be the same. Early in this study, it also became clear that Gaussians yield a much better fit than either Lorentzians or triangles.

Unless one has some *a priori* knowledge of the underlying physics, any profile decomposition is arbitrary, since it relies on certain assumptions which, in general, cannot be verified. For instance, one has to decide how many components need or must be included in the fit, which of the model parameters (intensities, widths, wavelengths) are free parameters representing time-variable quantities, and which are fixed. To answer such questions, we have been constantly guided by the following criteria:

1. A good fit must satisfy some basic statistical tests so as to ensure that the data are neither overinterpreted nor underinterpreted.
2. The number of free parameters must be kept to a minimum.
3. The model must be able to provide a good fit (in the sense of [1] for *all* epochs.
4. As far as possible, the model must bear a simple correspondence to the real world, i.e., the spectral components of the fit must be associated with physical quantities of easily recognized significance.

While our model satisfies the first three criteria, it only partially meets the fourth one. This is unfortunate but unavoidable, mainly because of the limited spectral resolution of the data as compared to the complexity of the actual line profiles when looked at with a higher dispersion (Penston *et al.* 1979). Our model should be regarded as a reliable filter which enables us to measure accurately the low-order moments of the profiles as a function of time. As mentioned in the introduction, we initially tried various kinds of semiphysical decompositions inspired by our crude subdivision into BLR1, BLR2, and BLR3 of Paper III. In the process, we thoroughly studied the C III λ1908 and Mg II λ2800 line profiles and their variations. Both features being narrower, we hoped to use them as guidelines in the decomposition of the more complex C IV λ1550 blend. This approach invariably failed. Moreover, it soon became obvious that every emission line displays its own specific profile which is distinct from that of the others. For instance, the C III λ1908 feature has most of its energy contained in a narrow core of constant width (1600 km s^{-1} FWHM) and whose intensity varies only on time scales of several months. Between 20% and 40% of its flux, however, originates in a broader (~7000 km s^{-1} FWHM) and more variable component. Since the latter is centered at 1900 Å, it presumably contains a ~50% contribution from Si III] λ1892, and the intrinsic width of the broad C III] feature alone is therefore of the order of 3500 km s^{-1}. The FWHM of the broad He II λ1640 line is 8600 km s^{-1}, clearly different from that of either the broad C III] or the broad C IV line. Our tests show that the Mg II λ2800 line profile is again different, while the shape of the Lyα λ1216 line is clearly distinct from that of the other UV lines as well as from that of the Balmer lines (Penston *et al.* 1979). In our opinion, this complex situation reflects the existence of a gradient of physical conditions and velocity dispersion acrosss the BLR of NGC 4151, each line emitting the bulk of its energy at a specific distance from the continuum source where these conditions are the most appropriate. It is therefore not surprising that our crude decomposition into BLR1, BLR2, and BLR3 fails to provide an adequate representation of the C IV profile.

Figure 1 provides some additional support to our model. It shows the difference spectrum of NGC 4151 obtained by subtracting an intermediate state (1979 May 3) from a bright state (1979 June 1). The various broad and variable components which have been mentioned earlier are clearly visible in this difference spectrum, while the nearly constant narrower spectral features—N IV] λ1485, He II λ1640–C, O III] λ1663, C III] λ1908–C—cancel out.[10] Among the broad emission components, He II λ1640–B and C IV–B are the most conspicuous. The weaker C III] λ1908 broad line is also visible, probably blended with Si III] λ1892.

b) *Description of the Method*

The computer code is essentially that of Pelat and Alloin (1980), with some minor technical improvements. Least-squares fitting techniques are used to adjust the free parameters of the model so as to minimize the residuals. The iterations are stopped when the fluctuations in the residuals are comparable to the noise in the spectra.

The profile of each of the various spectral components is represented by a Gaussian function and is therefore fully described by three parameters: its peak intensity, I_0 (in units of 10^{-13} ergs cm^{-2} s^{-1} Å^{-1} throughout), central wavelength, L_0 (in Å; always expressed in the rest frame of NGC 4151) and full width at half-maximum, (FWHM km s^{-1}). No correction for instrumental broadening was performed. The continuum is approximated by a straight line connecting the 1430–1470 Å and 1700–1720 Å spectral intervals. Its intensities at both wavelengths, $F(1450)$ and $F(1710)$, are free parameters of the model, together with the peak intensity, I_0 (or optical depth, T_0), wavelength L_0, and FWHM of the 10 different spectral components. For eight of these, the FWHMs have been fixed.

The C IV absorption is treated in a "multiplicative" way, i.e., at a given wavelength L, the total (emission plus absorption) intensity $I(L)$, is defined as:

$$I(L) = \sum [I_i(L)] \exp(-T_0) \exp[-(L - L_0)^2/2S^2],$$

where T_0, L_0, and S refer respectively to the "optical depth" at the line center, the wavelength, and the velocity dispersion

[10] The "C" in expressions like "He II λ1540–C" stands for "core," the "B" in expressions like "C IV–B" stands for "broad," and the "A" in expressions like "C IV–A" stands for "absorption."

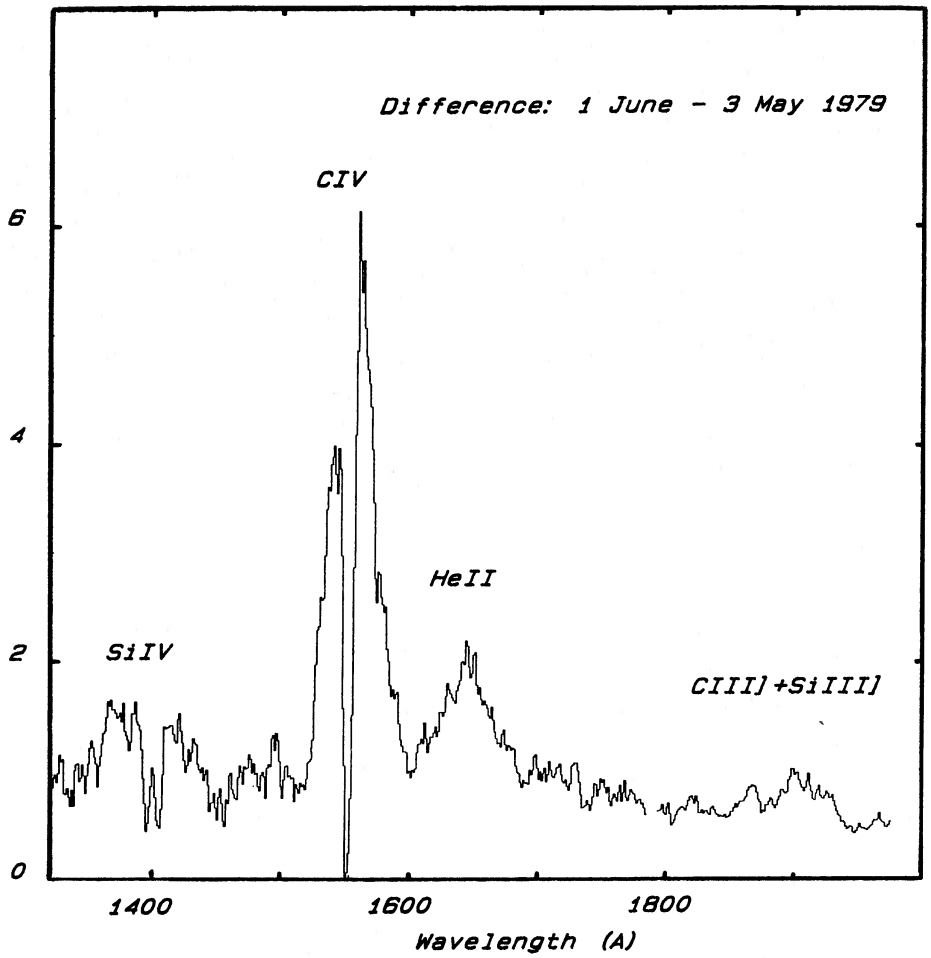

FIG. 1.—Difference spectrum obtained by subtracting spectrum of NGC 4151 on 1979 May 3 (intermediate state) from that recorded during high state of 1979 June 1. As is case for all figs; flux units are 10^{-13} ergs cm^{-2} s^{-1} Å^{-1}. Difference spectrum clearly shows broad and rapidly variable emission components which we refer to in text. On the other hand, narrow emission cores which vary little and only on long time scales cancel out. Apart from conspicuous broad He II and C IV feature, note presence of weaker broad lines, in particular one which can be attributed to blend of C III] λ1908 with Si III] λ1892.

(FWHM = 2.3543S) of the absorption feature, and the summation is carried over the 10 emission components (nine for the lines and one for the continuum) which contribute to the flux at L. Such a procedure is physically realistic in contrast to the method of Veron, Veron-Cetty, and Tarenghi (1985), for example, who deal with the absorption as if it were "negative" emission (i.e. who merely subtract a Gaussian line). Our method implicitly assumes that *both* the continuum and the emission lines are absorbed, an assumption which is supported by the existing five low–signal-to-noise ratio, high-resolution (20 km s^{-1}), far-UV spectra of NGC 4151 (Penston *et al.* 1979 and Paper IV). The absorption line is displaced by ~ -800 km s^{-1} with respect to the systemic velocity of NGC 4151 (Papers I and IV). Seen at high resolution, it is roughly trapezoidal and has a flat bottom. Because its width is only about twice the doublet separation, both the λ1548.2 and the λ1550.8 fine-structure components have been included in the fit. However, the λ1550.8 excited line is completely subordinated to the resonance line since (1) its optical depth, T_0' was arbitrarily set to $T_0' = 0.7T_0$, where T_0 is the optical depth of the λ1548.2 feature; (2) its wavelength L_0' is set proportional to that L_0 of the λ1548.2 line, $L_0' = (1550.8/1548.2)L_0$; (3) its FWHM is set equal to that of the resonance component. In this way we obtain a better representation of the trapezoidal shape of the C IV absorption trough without increasing the number of free parameters.

The rather weak "satellite" lines were not detected prior to the low state of 1980 April 13, presumably because the source had always been bright until then (at least for *IUE*), so that the very strong C IV wings overwhelmed them. Nevertheless, our models allow for their presence even for the epochs when they are not visually recognizable. All the other features stand out clearly at any epoch.

In Table 1 we summarize the characteristics of the model. In columns (1) and (2) we list the various spectral components and their associated parameters; in column (3), we indicate for each parameter whether it was free to vary with epoch, while in column (4) we list its value if it was fixed. There are 21 free parameters, for a total of 230 extracted data points corresponding to 60 resolution elements in the 1450–1720 Å spectral interval.

After convergence has been achieved, the residuals are compared to the noise in the data as obtained by measuring the standard deviation of the signal in the 1450 and 1710 Å continuum windows. Ideally, the two distributions should have the same standard deviation (χ^2 test) and cumulative probability distributions (Kolmogorov test). The distribution of the noise, however, and its amplitude as a function of the signal strength

are not known. In applying the χ^2 and Kolmogorov tests, the program implicitly assumes that the noise has a Gaussian distribution and scales as the square root of the signal, which is truly valid only in the case of pure photon noise. In fact, the characteristics of the *IUE* noise are poorly known, but differ substantially from that of photon noise, since (1) the original photoelectron events recorded by the *IUE* camera have suffered several manipulations, in particular their transformation into absolute flux and the averaging of individual spectra; (2) the *IUE* detectors have read-out noise and are nonlinear at high-level signals (i.e., at the top of the C IV emission line); and (3) the *IUE* noise includes fixed-pattern contributions which set an inherent limit to the highest possible signal-to-noise ratio achievable, for example, by averaging individual spectra. Typically, half of the noise in the continuum windows can be attributed to this fixed-pattern component for epochs when more than two NGC 4151 spectra are averaged.

It is worth stressing that, *within the adopted model*, the best-fit solutions are *unique*. In order to test the stability of the fit, these solutions were greatly perturbed and the iterating process was started again. In all cases, the program converges back to the previous best fitted solution.

c) *The Data Set*

We have analyzed all the *IUE* low resolution (900 km s^{-1}) SWP (1150–1950 Å) spectra of NGC 4151 up to 1983, inclusive. This represents a total of 69 different epochs. Most epochs consist of 4 hr (occasionally 8 hr) of continuous observation during which at least two (sometimes up to six) SWP spectra have been obtained. Since there are no variations on such short time scales (Paper II), a mean signal and rms noise spectra were computed. These average spectra, which together with the rms will be displayed in a forthcoming atlas (Snijders *et al.* 1987), form the data set studied here.

To remove the uncertainty inherent in the zero point of the *IUE* wavelength scale, the wavelength of the He II sharp core was used as a reference and assigned its laboratory value of 1640.5 Å.

Table 2 contains the log of the observations: the first and second columns give the dates and corresponding Julian days (JD −2,440,000.5), respectively. The third column lists the number of individual spectra averaged at each epoch, together with their exposure times.

d) *Errors in the Parameters and Goodness of the Fit*

For a subset of 19 epochs, chosen to be representative because of their signal-to-noise ratio and/or the brightness of the nucleus, the individual spectra were analyzed as well as the average spectra. The standard deviations of the best-fit values for individual spectra yielded reliable estimates of the uncertainty attached to each parameter for this subset of epochs. For the remaining epochs, the errors have been computed by scaling these values according to the signal-to-noise ratio of the fit. The "signal" was taken as the mean of $F(1450)$ and $F(1710)$ and the "noise" was the mean standard deviation of the residuals to the fit at the same wavelengths.

To assess the reality of the results, the program compares the residuals from the fit to the noise in the data. Estimates of the noise are provided by the standard deviations of the signal in the 1450 and 1710 Å continuum intervals. Similar quantities are obtained for the residuals from their rms fluctuations. The ratio of these two parameters defines what we call here the model-to-data noise ratio and is given in column (4) of Table 2, with its associated error. Column (5) lists the reduced χ^2, i.e., the result of comparing the rms fluctuations from the model to the initial noise estimate for all data points. Column (6) gives a significance level from the Kolmogorov test which compares the distribution of these residuals to an error function with this noise estimate as standard error.

It is reassuring that the fit residuals have fluctuations whose amplitude and distribution are consistent with those of the noise in the data. Indeed, the model-to-data noise ratio (col. [4]) averaged over the 69 epochs is 1.04 ± 0.27, which gives us some confidence that we have neither been overinterpreting nor underinterpreting the data. The rms residuals obtained from the process of averaging individual spectra provide another independent estimate of the noise in the data to be compared with the residuals from the fit such as those of Figure 2. This last check could only be done for a small subset of epochs (since the rms residuals became available only at a late stage of the present work) but essentially confirms that the residuals from the fit are very similar to the noise in the data, both in amplitude and distribution.

III. RESULTS

The best-fit parameters are given as a function of Julian day in Table 3 (continua), Table 4 (broad C IV and He II emission components), Table 5 (the C IV emission core and absorption lines), Table 6 (the C IV "satellite" L1, L2, and L'2 lines), and Table 7 (N IV] λ1485, He II λ1640 core, and O III] λ1663).

Figure 2 gives two examples of the fit when the nucleus is in a "bright" (Fig. 2*a*) and "low" (Fig. 2*b*) state.

a) *The Continuum*

The continuum varied by a factor of up to 10 in the entire 1978–1983 episode. Rapid variability was observed in several occasions, e.g., 1979 May, as was noted in our previous work (Paper II).

Figure 3 displays the continuum intensity at 1450 Å, $F(1450)$, versus the 1710 Å flux, $F(1710)$. This shows an excellent correlation between the two quantities. Indeed, a linear-regression analysis yields a correlation coefficient $r = 0.984$ and a reduced $\chi^2 = 0.57$ which implies that the correlation is significant at the 99.95% level of confidence.

Note that, throughout, the regression techniques which were used take into account *simultaneously* the errors in both variables, and therefore minimize the true distance to the regression line (York 1966), in contrast with the usual method which minimizes the distance along the y-axis only. The best-fit regression line is defined by

$$F(1710) = (0.747 \pm 0.015)F(1450) + (0.002 \pm 0.011) .$$

This means that, should $F(1450)$ vanish, $F(1710)$ would disappear as well. Moreover, it implies that while the continuum intensity varies, its spectral index ($F_\nu \approx \nu^\alpha$) remains constant:

$$\alpha = -0.17 \pm 0.12 .$$

Column (4) of Table 3 lists the value of the spectral index for each epoch. The mean (and error on the mean) of all epochs is -0.19 ± 0.15. None of the individual α deviates by more than 1.5 σ from the mean, and the usual tests show that the spectral index is constant at the 99% confidence level.

This mean value of α is interestingly close to that of the spectral index of the polarized optical continuum, $\alpha = -0.33$ (Schmidt and Miller 1980). The agreement remains good after

TABLE 2

INDICATORS OF THE QUALITY OF THE DATA AND OF THE FIT

Epoch	J.D. (a)	Nspec & Texp (b)	Residual/ Data-Noise (c)	χ^2 (d)	Kolmogorov test (e)
28 Feb 78	3568	1x120 (SWR)	1.07±0.0	1.23	>90 %
16 Apr 78	3615	2x40+20(S)	0.72±0.17	1.08	>90 %
17 Jun 78	3676	30(S)+80(S)	0.94±0.36	0.89	28 %
24 Jul 78	3714	60(S)+30	0.92±0.19	1.54	7 %
02 Aug 78	3722	30	1.28±0.65	1.50	>90 %
19 Oct 78	3801	30+25+60(S)	0.71±0.22	0.67	>90 %
31 Oct 78	3813	50(S)	1.01±0.49	1.44	60 %
09 Dec 78	3851	30+60(S)	0.90±0.09	1.97	>90 %
21 Jan 79	3895	2x25+60(S)	1.18±0.26	1.46	67 %
03 May 79	3996	3x25	0.94±0.18	0.93	>90 %
04 May 79	3998	20	1.13±0.39	1.23	54 %
19 May 79	4012	2x32+2x50+25+28	1.23±0.36	1.52	40 %
21 May 79	4014	2x30+50	1.09±0.26	1.23	68 %
23 May 79	4016	4x30	0.89±0.32	0.81	31 %
25 May 79	4018	2x30+50	1.30±0.30	1.77	30 %
31 May 79	4025	30	1.36±0.91	1.48	71 %
01 Jun 79	4025	5x25	1.20±0.31	1.22	79 %
08 Aug 79	4093	4x25+2x50	1.06±0.10	1.22	89 %
07 Dec 79	4215	3x25+3x15(m)	1.87±0.91	3.09	53 %
12 Dec 79	4220	2x25+50&42(S)	1.40±0.15	2.12	57 %
13 Dec 79	4220	4x25+15	1.71±0.06	3.30	25 %
01 Jan 80	4239	3x25+50(S)	1.52±0.40	2.39	39 %
01 Mar 80	4299	25+43	0.90±0.34	0.77	>90 %
04 Mar 80	4302	2x25	0.94±0.40	1.34	>90 %
06 Mar 80	4304	25	0.71±0.05	0.56	>90 %
13 Apr 80	4342	17	0.89±0.32	0.75	>90 %
21 Apr 80	4350	25+37.5+25(s)	1.60±0.77	2.56	80 %
15 May 80	4374	40	1.00±0.01	1.09	>90 %
19 May 80	4378	2x25+47	1.08±0.17	1.25	>90 %
29 Jul 80	4449	15	1.02±0.28	1.04	54 %
26 Nov 80	4569	3x35(m)	2.00±0.60	2.46	52 %
26 Apr 81	4720	25+40	0.92±0.34	0.83	5 %
30 Apr 81	4724	25+50	0.93±0.18	0.89	24 %
04 May 81	4728	25+40+60	0.95±0.13	0.98	38 %
08 May 81	4732	154	1.15±0.18	1.43	32 %
12 May 81	4736	25+40	1.16±0.01	1.47	>90 %
17 May 81	4741	30+120	1.00±0.40	0.92	>90 %
23 May 81	4747	30+120	0.96±0.13	0.98	83 %
25 May 81	4749	50	1.00±0.36	0.96	30 %
30 May 81	4754	30+120	0.78±0.08	0.66	57 %
05 Jun 81	4760	30+96	1.09±0.26	1.21	86 %
08 Jun 81	4764	30+120	0.87±0.10	0.82	>90 %
25 Jun 81	4781	30	0.90±0.12	0.87	>90 %
27 Jun 81	4783	30	0.99±0.07	1.07	>90 %
29 Jun 81	4785	30	0.85±0.32	0.68	11 %
03 Jul 81	4789	25	0.88±0.05	0.83	20 %
06 Jul 81	4792	60	0.73±0.18	0.53	19 %
16 Jul 81	4802	30+100	0.86±0.08	0.79	>90 %
27 Jul 81	4813	30	0.72±0.10	0.55	85 %
20 Feb 82	5020	50	1.52±1.12	1.34	76 %
26 Feb 82	5026	45	0.96±0.34	0.90	24 %
28 Feb 82	5029	45	1.08±0.35	1.13	59 %
17 Apr 82	5077	69+90	0.99±0.13	1.04	>90 %
18 Apr 82	5078	15+15	1.01±0.14	1.08	76 %
06 Nov 82	5280	25+45	1.14±0.12	1.40	>90 %
28 Dec 82	5331	105	1.17±0.05	1.48	>90 %
17 Mar 83	5410	30+70	0.96±0.09	0.98	85 %
20 Mar 83	5413	30+101	0.92±0.03	0.90	54 %
24 Mar 83	5417	30+60	1.05±0.45	1.00	>90 %
27 Mar 83	5420	30+60	0.82±0.19	0.69	46 %
16 May 83	5471	12	0.37±0.10	1.25	77 %
17 May 83	5472	17	1.06±0.22	1.20	>90 %
18 May 83	5473	20	0.84±0.14	0.75	>90 %
30 Oct 83	5638	50+40	1.05±0.18	1.17	7 %
04 Nov 83	5643	50+50	0.76±0.04	0.63	>90 %
07 Nov 83	5646	65+45	0.84±0.06	0.76	26 %
11 Nov 83	5650	66+45	0.78±0.23	0.59	39 %
15 Nov 83	5654	60+50	0.99±0.20	1.03	68 %
19 Nov 83	5658	120	0.91±0.28	0.80	25 %

NOTE.—Cols. (a)–(e) are as follows: (a) Julian Date −2,440,000.5. (b) Number of SWP spectra and their exposure time in minutes; an "S" means the spectrum was obtained through the small aperture, and "SWR" that it was recorded with the redundant camera; "m" is a multiple exposure. (c) Ratio of the noise in the residual of the fit to the noise in the data. (d) Reduced χ^2. (e) Confidence level of the Kolmogorov test.

correction for reddening; using $E(B-V) = 0.05$ (Paper II) and the Seaton (1979) law, the spectral indices become −0.02 and −0.16 for the UV and polarized continuum, respectively. For wavelengths greater than 2000 Å, the continuum is definitely steeper ($\alpha = -1.5$ to -3.5; Paper II), which probably reflects the fact that Balmer continuous emission and blended low-contrast Fe II lines contaminate the spectrum in the ~2000–4000 Å range (Wills, Netzer, and Wills 1985).

b) *The Broad* C IV *Emission Component*

The broad (FWHM = 14,600 km s^{-1}) component of the C IV λ1550 emission line, C IV–B, has a fractional range of variation comparable to that of the continuum (factor of ~10) and occasionally varies on a time scale of a few days as well.

Figure 4 displays the intensity of the broad C IV emission component, I_0(C IV–B), versus F(1450). The two quantities are *not* independent at the 99.9% confidence level. However, an

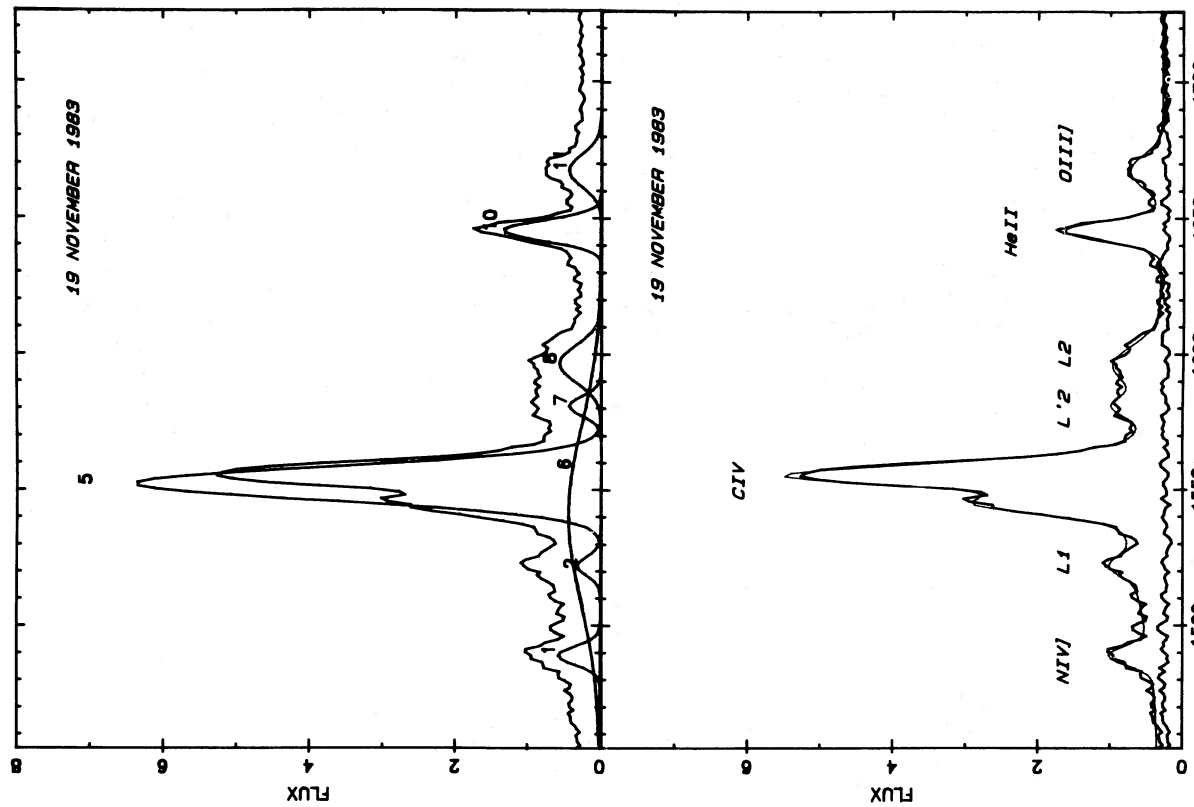

FIG. 2b

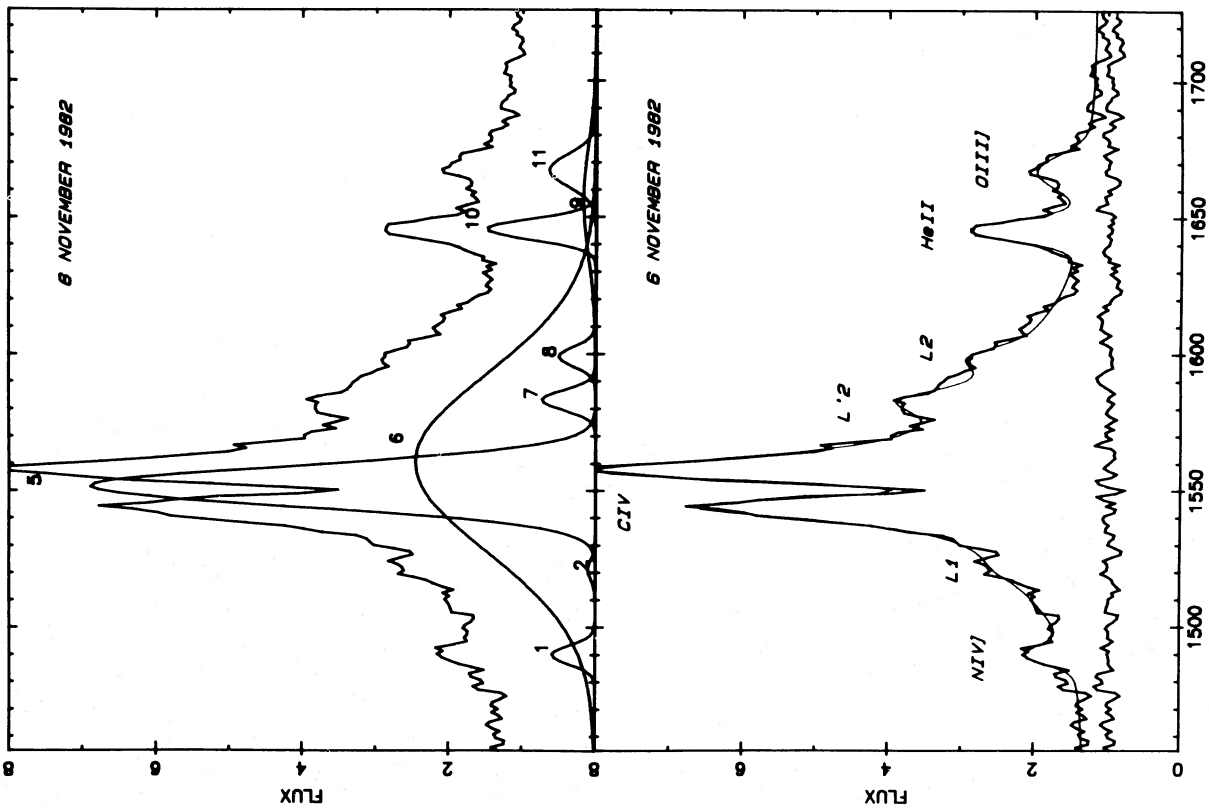

FIG. 2a

FIG. 2.—The 1450–1720 Å spectral region of NGC 4151 at two different epochs, when nucleus is in a "high" (*a*) and a "low" (*b*) state of brightness. Lower panels show best-fit models (*thin line*) on top of original data (*heavy line*), while in upper panels are displayed various spectral components of fit. Continuum and absorption lines omitted for clarity. Components are numbered according to order of appearance in Table 1. Various features are identified in lower panels, where are also shown residuals from fit. These residuals have been "normalized" to level of continuum and divided by square root of strength of signal, i.e., photon noise component has been "taken out" for illustrative purposes. Wavelengths are *not* corrected for systemic velocity of galaxy.

TABLE 3

THE BEST-FIT CONTINUUM INTENSITY AT 1450 AND 1710 Å AND SPECTRAL INDEX α

J.D.	F(1450)	F(1710)	α
	(10^{-13} erg.cm^{-2}.s^{-1}.A^{-1})		
3568	2.180±0.200	1.830±0.180	−0.90±1.20
3615	2.384±0.200	1.764±0.170	−0.11±1.13
3676	1.991±0.190	1.437±0.170	0.05±1.34
3714	1.513±0.120	1.110±0.100	−0.05±1.06
3722	1.524±0.160	1.031±0.130	0.46±1.45
3801	1.488±0.100	1.203±0.100	−0.66±0.95
3813	0.483±0.130	0.426±0.120	−1.21±3.45
3851	1.117±0.100	1.069±0.090	−1.72±1.09
3895	0.826±0.110	0.540±0.090	0.67±1.89
3996	1.229±0.120	0.687±0.100	1.66±1.53
3998	1.030±0.230	0.520±0.180	2.30±3.58
4012	1.934±0.130	1.425±0.110	−0.08±0.91
4014	2.068±0.120	1.555±0.110	−0.21±0.81
4016	2.058±0.110	1.522±0.090	−0.10±0.71
4018	2.080±0.130	1.613±0.110	−0.40±0.82
4025	2.152±0.250	1.612±0.210	−0.18±1.55
4025	2.060±0.140	1.610±0.130	−0.45±0.93
4093	1.250±0.100	0.960±0.090	−0.34±1.09
4215	1.601±0.110	1.350±0.100	−0.93±0.90
4220	1.233±0.100	0.985±0.090	−0.59±1.08
4220	1.210±0.100	0.954±0.090	−0.51±1.11
4239	1.270±0.120	0.920±0.100	0.03±1.28
4299	1.030±0.080	0.640±0.070	0.99±1.18
4302	1.170±0.130	0.760±0.100	0.71±1.53
4304	1.390±0.130	0.870±0.110	0.95±1.38
4342	0.409±0.080	0.257±0.060	0.92±2.70
4350	0.380±0.060	0.240±0.050	0.89±2.30
4374	2.031±0.160	1.293±0.130	0.84±1.13
4378	1.840±0.110	1.420±0.090	−0.37±0.77
4449	0.654±0.220	0.557±0.180	−0.99±4.15
4569	0.192±0.090	0.170±0.090	−1.23±6.28
4720	0.121±0.070	0.178±0.060	−4.43±5.76
4724	0.185±0.080	0.140±0.050	−0.25±4.96
4728	0.199±0.060	0.164±0.050	−0.78±3.81
4732	0.230±0.050	0.170±0.040	−0.10±2.85
4736	0.231±0.060	0.153±0.050	0.59±3.69
4741	0.289±0.050	0.190±0.040	0.64±2.41
4747	0.310±0.050	0.239±0.040	−0.36±2.07
4749	0.200±0.090	0.180±0.080	−1.34±5.62
4754	0.287±0.050	0.200±0.040	0.27±2.35
4760	0.308±0.060	0.215±0.050	0.26±2.69
4764	0.287±0.050	0.215±0.040	−0.18±2.26
4781	0.320±0.090	0.220±0.080	0.36±4.05
4783	0.200±0.090	0.220±0.080	−2.60±5.12
4785	0.260±0.090	0.220±0.070	−0.95±4.18
4789	0.144±0.080	0.156±0.080	−2.50±6.72
4792	0.253±0.060	0.186±0.050	−0.07±3.18
4802	0.214±0.050	0.197±0.050	−1.48±3.06
4813	0.084±0.070	0.128±0.060	−4.65±8.19
5020	0.650±0.080	0.327±0.060	2.32±1.93
5026	0.519±0.080	0.284±0.060	1.79±2.30
5029	0.724±0.130	0.401±0.100	1.71±2.70
5077	1.184±0.110	0.773±0.090	0.68±1.32
5078	1.025±0.150	0.676±0.120	0.62±2.04
5280	1.343±0.100	1.189±0.090	−1.23±0.94
5331	1.249±0.100	0.886±0.080	0.16±1.07
5410	0.565±0.060	0.411±0.050	0.00±1.43
5413	0.537±0.060	0.367±0.050	0.39±1.56
5417	0.648±0.070	0.456±0.060	0.21±1.51
5420	0.493±0.070	0.366±0.040	−0.13±1.58
5471	1.300±0.350	0.757±0.280	1.40±4.02
5472	1.344±0.350	0.756±0.280	1.62±3.97
5473	1.149±0.160	0.907±0.150	−0.51±1.92
5638	0.629±0.080	0.547±0.070	−1.12±1.60
5643	0.478±0.060	0.387±0.050	−0.67±1.60
5646	0.436±0.070	0.346±0.060	−0.55±2.10
5650	0.329±0.050	0.278±0.050	−0.94±2.09
5654	0.326±0.060	0.247±0.050	−0.26±2.43
5658	0.340±0.050	0.280±0.040	−0.78±1.82

F-test confirms the intuitive impression conveyed by Figure 4, namely that a linear dependence is not (at the 99.9% level) the optimal regression. For the sake of clarity and in the absence of an obviously better choice, we have nevertheless retained the linear approximation. A regression analysis yields $r = 0.844$, a reduced χ^2 of 6.0 (the correlation is clearly imperfect), and

$$I_0(\text{C IV–B}) = (1.064 \pm 0.022)F(1450) + (0.075 \pm 0.012) .$$

As noted in Papers I and III, the tight relation between these two parameters gives strong support to models where the broad-line intensities of AGNs are governed by the rate of continuum photoionization. In the framework of such models, correlations between the line and continuum strengths will be weakened because of the time required for the ionizing photon to propagate through the BLR. In such a context, the above correlation is astonishingly good and indicates that the propagation time must be comparable to the time scale of variation.

This is supported by Figures 5*a*–5*c* where the light curves of the continuum and C IV–B are plotted one on top of the other for the three best sampled events, the 1979 May–June outburst, the 1983 October–November decay, and the 1981 April–July fluctuations. These episodes suggest time delays of 0 to 15, 4, and 4 to 11 days, respectively. In the Appendix we explain why cross-correlation (CC) techniques fail to improve upon these intuitive figures. For reference, we show in Figure 5*d* the CC function of the entire 1978–1983 continuum and C IV–B light curves and note that its maximum occurs at −9 days, in rough agreement with the "visual" estimates. Our best estimate of the response time of the C IV–B emitting region to the variations in the continuum intensity is $5 + 4/ - 2$ days.

Additional information is provided by a comparison of the largest rate dI/Idt of variation of I_0(C IV–B) and F(1450). Let us define it as

$$dI/Idt = (I_1 - I_2)/I_1\Delta t ,$$

where I_1 and I_2 are the intensities at epoch 1 and 2, respectively, and Δt is the elapsed time. The 1979 May 3–19 outburst and the 1983 October 30–November 19 decay yield the same value $dI/Idt \approx 4\%$ per day both for the continuum and the C IV–B line.

Let us now assume the simplest possible model, where a geometrically thin shell of radius R is ionized by a point-like central continuum source and reemits those photons in the form of broad spectral lines. Photon reprocessing by the shell yields a light curve which closely mimics that of the continuum (somewhat blurred) but is translated along the time axis by R/c. Moreover, after a transition phase (which lasts $2R/c$), the rate of increase/decrease is the same for the continuum and the line (Blandford and McKee 1982). The delay has a purely geometric origin since the recombination time is shorter than 1000 s at the high BLR densities. It represents the *average* excess distance which a photon reverberated by the shell has to travel as compared to a continuum photon which reaches the observer directly. The results above are plainly consistent with such a simple model and suggest that the bulk of the broad C IV emitting gas lies at ~5 lt-day from the continuum source. Hereafter, such a distance will (abusively) be called "radius" for simplicity. Two folding time scales (Paper II) by definition can only yield upper limits R_{max} to the true radius. Nevertheless, it is interesting that the most rapid rise (1980 April 21–May 19) and decay (1983 November 11–15) yield respectively $R_{max} = 10 \pm 2$ and 5 ± 1 lt-day, in good agreement with the above estimate.

Figure 6*a* displays the wavelength of the broad C IV component, L_0(C IV–B), versus its intensity. A clear trend is apparent, with L_0(C IV–B) increasing with I_0(C IV–B). The usual tests show that the two variables are *linearly* related at the 99.9% confidence level ($r = 0.67$). The correlation is not perfect since a linear fit to the data yields a reduced χ^2 of 3.4. Because this correlation has important implications, we have carefully examined the possibility that it is spurious. Several artifacts could conceivably mimic an intensity-dependent asymmetry of the C IV line.

TABLE 4

BEST-FIT PARAMETERS FOR THE BROAD C IV AND He II LINES

J.D.	CIV λ1550 BROAD Io.10^{-13} (erg/cm^2/s/A)	CIV λ1550 BROAD Lo-1500 (A)	HeII λ1640 BROAD Io.10^{-13} (erg/cm^2/s/A)	HeII λ1640 BROAD Lo-1500 (A)
3568	1.70±0.15	41.9±3.0	0.48±0.08	35.5±2.0
3615	3.36±0.30	44.8±3.0	0.58±0.09	48.9±2.0
3676	2.44±0.20	47.7±3.0	0.78±0.13	50.5±3.0
3714	1.80±0.20	39.7±3.0	0.33±0.06	50.5±2.0
3722	1.29±0.15	36.2±4.0	0.23±0.05	50.5±2.5
3801	3.21±0.30	41.1±3.0	0.84±0.13	50.5±2.0
3813	1.64±0.23	39.2±5.0	0.29±0.07	50.5±3.5
3851	2.20±0.18	43.4±3.0	0.48±0.08	43.9±2.0
3895	0.69±0.06	30.5±2.5	0.25±0.04	55.5±2.0
3996	1.13±0.10	35.2±2.4	0.00	...
3998	1.18±0.15	44.6±3.9	0.00	...
4012	1.70±0.15	41.5±2.0	0.48±0.08	41.1±2.0
4014	1.70±0.15	46.1±1.8	0.58±0.09	39.8±2.0
4016	1.72±0.15	45.4±1.8	0.68±0.11	41.3±2.0
4018	1.66±0.15	42.5±1.9	0.68±0.11	40.5±2.0
4025	1.94±0.30	48.9±3.0	0.90±0.25	42.5±3.0
4025	1.73±0.14	47.6±2.8	0.86±0.14	42.7±2.0
4093	1.10±0.09	37.6±2.8	0.42±0.07	42.3±2.0
4215	2.03±0.16	47.3±2.8	0.63±0.10	35.5±2.0
4220	1.99±0.16	42.7±2.8	0.68±0.11	43.3±2.0
4220	1.98±0.16	42.8±2.8	0.65±0.10	44.2±2.0
4239	1.50±0.12	41.1±2.3	0.51±0.07	36.5±1.8
4299	1.07±0.10	36.8±2.1	0.22±0.03	50.0±2.0
4302	0.77±0.07	38.7±2.5	0.16±0.03	34.2±2.0
4304	0.90±0.07	44.5±2.2	0.21±0.03	30.5±1.7
4342	0.46±0.05	41.9±3.2	0.00	...
4350	0.27±0.03	31.2±2.8	0.00	...
4374	1.26±0.12	50.2±2.8	0.37±0.07	55.5±2.7
4378	1.54±0.13	48.5±2.8	0.37±0.05	47.1±1.9
4449	1.21±0.13	49.5±5.0	0.14±0.04	50.0±3.5
4569	0.17±0.04	33.3±4.3	0.00	...
4720	0.38±0.05	32.1±3.6	0.00	...
4725	0.37±0.04	31.6±3.3	0.00	...
4728	0.26±0.03	31.2±3.0	0.00	...
4732	0.23±0.02	36.7±2.6	0.00	...
4736	0.26±0.03	32.5±2.8	0.00	...
4741	0.29±0.02	31.5±2.3	0.00	...
4747	0.34±0.03	30.5±2.2	0.00	...
4749	0.40±0.05	34.9±3.5	0.00	...
4754	0.28±0.02	33.3±2.8	0.00	...
4760	0.31±0.03	31.3±3.0	0.00	...
4764	0.36±0.03	30.5±2.8	0.00	...
4781	0.47±0.05	30.6±3.5	0.00	...
4783	0.58±0.07	30.5±4.0	0.00	...
4785	0.40±0.04	30.5±3.8	0.00	...
4789	0.50±0.07	30.5±4.5	0.00	...
4792	0.41±0.04	31.3±3.2	0.00	...
4802	0.34±0.04	35.7±3.2	0.00	...
4813	0.41±0.06	31.8±4.5	0.00	...
5020	0.57±0.05	31.6±2.6	0.00	...
5026	0.44±0.04	31.2±2.6	0.00	...
5029	0.55±0.05	30.5±2.8	0.00	...
5077	0.95±0.07	49.5±2.1	0.00	...
5078	0.85±0.08	48.2±2.6	0.00	...
5280	2.45±0.16	55.5±1.9	0.17±0.02	50.5±2.0
5331	1.43±0.10	50.5±2.0	0.13±0.02	50.5±2.0
5410	1.15±0.09	49.9±2.3	0.00	...
5413	1.05±0.09	45.4±2.3	0.00	...
5417	1.02±0.08	47.5±2.3	0.00	...
5420	0.82±0.08	48.2±2.7	0.00	...
5471	1.55±0.26	42.8±4.9	0.00	...
5472	1.33±0.20	48.6±3.3	0.00	...
5473	1.65±0.16	50.5±2.8	0.00	...
5638	1.54±0.14	47.3±2.6	0.00	...
5643	1.04±0.09	45.7±2.4	0.00	...
5646	0.81±0.08	43.9±2.8	0.00	...
5650	0.70±0.07	37.7±2.8	0.00	...
5654	0.39±0.04	38.5±3.0	0.00	...
5658	0.44±0.04	36.2±2.7	0.00	...

A first possibility is that a weak constant or slowly varying emission feature is hidden in the C IV blue wing, its influence becoming noticeable only when the source is faint. The only plausible candidate is Si II λ1526.7, 1533.4 (UV2). To lower the wavelength of the C IV–B component artificially, it should carry at least one-fourth of its total residual flux at low state, i.e., 8×10^{-13} ergs cm^{-2} s^{-1}. This is about the maximum intensity achieved by the clearly recognizable N III] λ1750 emission feature and is definitely much larger than the intensities of either the Si II λλ1260, 1265 (UV4) or Si II λλ1808, 1817 (UV1) multiplets. The UV1 line is theoretically stronger than that of UV2 at low temperatures, while the UV4 line dominates at high temperatures. However, both the UV1 and UV4 lines are extremely weak and hardly stand above the noise level in the average of all low-state NGC 4151 spectra (Snijders *et al.* 1987). The intensity of UV1, for instance, is at most 10^{-13} ergs cm^{-2} s^{-1}, and Si II UV2 can therefore be ruled out as the cause of the L_0(C IV–B)/I_0(C IV–B) correlation. Moreover,

TABLE 5

FREE PARAMETERS OF THE FIT FOR THE C IV ABSORPTION LINE AND EMISSION CORE

J.D.	CIV Absorption			CIV 1549.5 Emission Core		
	To	Lo-1540 (A)	Eq.Width (A)	Io*10-13 (erg/cm2/s/A)	Lo-1500 (A)	FWHM (km.s-1)
3567	0.59±0.03	7.3±1.0	5.5±0.5	07.3±0.8	48.0±0.5	4170±100
3615	0.57±0.03	5.8±1.0	5.7±0.5	08.0±1.0	48.9±0.5	4400±200
3676	0.70±0.04	7.2±0.7	6.3±0.6	10.0±0.7	49.4±0.6	5220±130
3714	0.57±0.03	4.8±1.0	5.6±0.5	09.5±0.7	49.9±0.5	4360±110
3722	0.46±0.02	4.6±1.0	4.7±0.4	08.0±0.6	50.5±0.5	4910±130
3801	0.60±0.03	5.4±0.7	5.7±0.5	09.7±0.4	51.5±0.5	4830±130
3813	0.68±0.06	3.7±1.0	6.9±1.2	09.6±0.8	48.7±0.8	3490±100
3851	0.35±0.02	4.8±0.7	4.9±0.4	08.7±0.5	49.0±0.5	5540±140
3895	0.55±0.03	4.4±0.4	5.4±0.5	08.4±0.3	48.2±0.4	5160±130
3996	0.75±0.04	3.5±0.4	7.7±0.8	09.0±0.4	46.5±0.4	3260± 80
3998	0.75±0.07	4.0±0.7	7.3±1.4	08.7±0.6	47.4±0.8	3490±140
4012	0.71±0.04	4.8±0.4	6.6±0.6	09.0±0.4	47.5±0.4	4560±110
4014	0.70±0.04	4.5±0.4	6.5±0.6	09.2±0.4	47.2±0.4	4760±120
4016	0.76±0.04	4.7±0.4	6.8±0.7	09.9±0.4	47.3±0.4	4760±120
4018	0.72±0.04	4.6±0.4	6.5±0.6	09.5±0.4	47.2±0.4	5010±130
4025	0.76±0.07	5.4±0.7	6.8±1.2	10.1±0.7	48.4±0.7	4760±210
4025	0.76±0.04	4.7±0.4	6.4±0.6	10.3±0.4	47.5±0.4	4720±120
4093	0.72±0.04	4.1±0.4	6.8±0.7	09.6±0.4	48.2±0.4	3980±100
4215	0.70±0.04	4.2±0.4	6.3±0.6	09.6±0.4	48.1±0.4	4150±100
4220	0.82±0.04	5.6±0.4	7.4±0.8	10.4±0.4	49.6±0.4	3820±100
4220	0.75±0.04	5.3±0.4	6.9±0.7	09.7±0.4	49.2±0.4	3790± 90
4239	0.80±0.04	4.1±0.4	7.2±0.7	11.1±0.4	47.2±0.4	4140±100
4299	0.73±0.03	2.9±0.3	7.3±0.6	09.5±0.3	47.3±0.3	3300±100
4302	0.77±0.04	2.8±0.4	7.6±0.9	09.3±0.4	47.2±0.4	3550± 90
4304	0.70±0.03	3.0±0.4	7.0±0.6	09.1±0.3	47.1±0.4	3540± 90
4342	0.73±0.05	3.6±0.5	7.7±1.1	08.0±0.4	48.0±0.5	3380±110
4350	0.76±0.04	2.7±0.4	8.3±0.9	09.3±0.4	47.3±0.4	3100± 80
4374	sat	4.2±0.5	sat	sat	48.2±0.8	sat
4378	0.68±0.03	2.8±0.3	6.2±0.5	08.5±0.3	47.1±0.6	4100± 70
4449	<0.81±0.07	3.9±0.9	< 8.7±1.6	09.3±0.6	47.8±0.9	2600±100
4569	<0.82±0.08	4.1±1.0	< 9.3±2.0	08.0±0.6	48.8±1.0	2180±110
4720	<0.93±0.07	3.4±0.5	<10.2±1.8	08.9±0.4	47.2±0.5	2520±100
4724	<1.01±0.07	3.2±0.4	<10.8±1.8	09.3±0.4	47.1±0.4	2440± 90
4728	<0.93±0.06	3.1±0.4	<10.4±1.6	09.4±0.4	46.9±0.4	2440± 80
4732	sat	3.0±0.3	sat	09.2±0.3	47.0±0.6	sat
4736	<1.00±0.06	2.9±0.4	<10.5±1.5	08.7±0.3	47.1±0.4	2410± 80
4741	<0.98±0.05	3.3±0.3	<10.9±1.4	09.3±0.3	46.9±0.3	2380± 60
4747	<0.97±0.05	3.4±0.3	<10.6±1.3	09.5±0.3	46.4±0.4	2600± 60
4749	<1.08±0.08	3.0±0.5	<11.7±2.1	10.6±0.5	46.3±0.5	2450± 90
4754	<1.01±0.05	2.8±0.3	<11.3±1.4	10.3±0.3	46.2±0.3	2460± 60
4760	<0.96±0.05	3.3±0.3	<10.6±1.3	09.1±0.3	46.7±0.3	2550± 70
4764	<0.96±0.05	3.3±0.3	<10.8±1.3	09.6±0.3	46.7±0.3	2520± 60
4781	<0.88±0.06	4.0±0.4	< 9.9±1.5	09.6±0.4	47.2±0.4	2760± 90
4783	<0.87±0.06	3.4±0.4	< 9.9±1.6	09.1±0.4	47.0±0.4	2670±100
4783	<0.91±0.06	3.2±0.4	< 9.9±1.5	09.1±0.4	46.6±0.4	2810± 90
4789	<0.93±0.08	3.4±0.5	<10.2±2.0	09.7±0.5	46.8±0.5	2620±110
4792	sat	3.4±0.3	sat	sat	46.8±0.7	sat
4802	<0.94±0.06	3.4±0.4	<10.4±1.5	09.3±0.4	45.9±0.4	2510± 80
4813	<1.01±0.09	3.5±0.5	<10.7±2.3	09.3±0.5	47.6±0.6	2440±110
5020	<0.81±0.04	3.8±0.4	< 9.4±1.0	08.3±0.3	46.9±0.4	2520± 60
5026	<0.84±0.04	3.7±0.4	< 9.5±1.0	07.8±0.3	47.2±0.4	2610± 70
5029	<0.80±0.04	2.3±0.4	< 9.1±1.0	08.5±0.4	45.6±0.4	2720± 70
5077	<0.89±0.04	3.1±0.3	< 9.3±0.9	08.9±0.3	45.6±0.3	2800± 60
5078	0.72±0.04	3.6±0.4	7.7±0.9	07.5±0.3	46.8±0.4	3040± 80
5280	0.62±0.02	4.9±0.3	6.4±0.4	06.9±0.2	47.1±0.3	3340± 70
5331	sat	4.5±0.3	sat	sat	47.0±0.6	sat
5410	0.71±0.03	4.4±0.3	7.7±0.7	07.7±0.3	47.4±0.3	3000± 70
5413	<0.71±0.03	4.2±0.3	< 7.8±0.7	09.2±0.3	48.0±0.3	2890± 70
5417	<0.79±0.04	3.7±0.3	< 8.5±0.9	09.6±0.3	47.4±0.3	2840± 60
5420	<0.78±0.04	4.0±0.3	< 8.5±0.9	09.7±0.4	47.7±0.3	2840± 70
5471	<0.80±0.10	3.4±0.8	< 8.3±2.2	09.7±1.0	47.0±0.8	2820±260
5472	0.76±0.08	2.6±0.6	7.5±1.6	07.3±0.8	45.1±0.7	3190±200
5473	<0.86±0.05	3.5±0.4	< 8.8±1.1	09.0±0.4	46.5±0.4	2830± 70
5638	<0.75±0.04	4.5±0.3	< 8.1±0.9	08.6±0.4	47.4±0.3	2860± 70
5643	<0.76±0.04	4.2±0.4	< 8.7±1.0	09.0±0.3	47.3±0.4	2700± 60
5646	<0.80±0.04	3.8±0.4	< 9.0±1.0	09.1±0.4	47.2±0.4	2640± 70
5650	<0.74±0.04	3.8±0.4	< 8.6±1.0	08.5±0.4	47.5±0.4	2630± 70
5654	<0.79±0.05	3.6±0.5	< 8.9±1.2	08.4±0.4	47.6±0.5	2650± 80
5658	sat	3.7±0.8	sat	sat	47.5±0.9	sat

there is no *a priori* reason why the Si II line intensity should be constant, while features from similar ions, such as Mg II λ2800, vary in response to the continuum.

We have also looked into the possibility that the correlation is an artifact introduced by the profile fitting procedure itself. For instance, at low states the slope of the continuum could be systematically overestimated by the program, and the broad C IV line be shifted toward negative velocities so as to provide the missing short wavelength flux. If this was the case, the $F(1450)/F(1710)$ continuum intensity ratio would be lower when the C IV–B line is blueshifted. However, the mean value of $F(1450)/F(1710)$ averaged over the 34 epochs when $L_0(\text{C IV–B}) < 1540$ is 1.34 ± 0.30 and 1.35 ± 0.20 for the remaining 35 epochs. Moreover, a student's t-test shows that the two variables are independent at the 99.9% confidence level.

We were also concerned with the possibility that the program could systematically transfer some of the flux in the

TABLE 6

BEST-FIT PARAMETERS FOR THE L1, L2 and L'2 UNIDENTIFIED LINES

J.D.	L1λ1518		L2λ1594			L'2λ1576	
	Io.10^{-13} (erg/cm^2/s/A)	Lo-1510 (A)	Io.10^{-13} (erg/cm^2/s/A)	Lo-1590 (A)	FWHM (km.s^{-1})	Io.10^{-13} (erg/cm^2/s/A)	Lo-1570 (A)
3568	0.27±0.05	6.7±1.2	<0.52±0.19	5.5±2.0	1600±100	<0.72±0.32	3.7±2.0
3615	0.00	...	0.00	...	...	<0.92±0.40	2.5±2.0
3676	0.00	...	reseaux	...	...	reseaux	...
3714	0.00	...	<0.95±0.10	1.5±2.0	3000±280	<1.06±0.46	3.7±2.0
3722	0.00	...	1.06±0.10	2.2±2.0	2920±300	<1.05±0.46	7.9±2.0
3801	<0.64±0.13	5.2±1.2	0.00	...	...	<0.53±0.23	6.8±2.0
3813	0.00	...	0.00	...	...	reseaux	reseaux
3851	<0.85±0.17	5.5±1.2	0.00	...	...	<0.27±0.12	2.5±2.0
3895	<0.55±0.12	7.1±1.2	<0.77±0.13	1.5±2.0	2580±250	<0.46±0.18	7.6±1.8
3996	0.34±0.08	5.9±0.9	0.43±0.04	3.3±1.0	1600±100	<0.22±0.08	1.5±1.5
3998	<0.50±0.15	6.1±1.3	0.29±0.03	2.5±1.0	1600±100	<0.20±0.10	9.0±2.3
4012	<0.13±0.03	7.0±1.0	<0.14±0.03	4.6±1.5	1600±100	<0.47±0.14	6.0±1.3
4014	<0.33±0.05	8.0±0.8	0.00	...	...	<0.41±0.12	6.2±1.3
4016	<0.23±0.04	9.0±0.8	0.00	...	...	<0.56±0.16	5.5±1.3
4018	<0.41±0.06	6.0±1.0	<0.18±0.03	5.5±1.7	1600±100	<0.71±0.22	6.9±1.4
4025	<0.16±0.03	9.0±1.2	0.00	...	...	<0.72±0.28	6.4±1.8
4025	<0.20±0.03	7.6±1.0	<0.12±0.03	2.5±1.8	1600±100	<0.82±0.26	6.3±1.4
4093	<0.46±0.10	7.8±1.2	<0.10±0.03	5.3±1.4	1600±100	<0.35±0.12	4.2±1.5
4215	<0.10±0.03	5.0±1.2	<0.43±0.06	5.5±1.7	1600±100	0.00	...
4220	0.00	...	<0.44±0.06	4.4±1.5	1600±100	0.00	...
4220	0.00	...	<0.49±0.07	5.5±1.8	1600±100	0.00	...
4239	<0.38±0.07	9.0±1.2	<0.36±0.06	5.5±1.0	3000±300	<0.41±0.16	6.0±1.8
4299	0.00	...	0.57±0.05	5.5±0.8	1870±150	0.00	...
4302	<0.19±0.07	5.3±1.6	0.73±0.06	6.1±1.0	2680±150	<0.38±0.16	9.9±2.0
4304	<0.20±0.08	3.8±1.5	0.66±0.06	4.2±1.0	1920±150	0.40±0.08	9.9±1.5
4342	<0.10±0.05	9.0±2.5	0.42±0.05	3.8±1.3	1600±200	<0.05±0.03	9.0±2.5
4350	0.28±0.06	6.1±0.7	0.34±0.03	5.5±1.0	1600±100	<0.15±0.07	1.5±2.0
4374	0.67±0.16	5.4±1.0	0.60±0.07	4.0±1.4	1600±100	<0.33±0.19	2.5±2.7
4378	0.42±0.06	5.7±0.6	<0.33±0.06	5.5±1.7	1600±100	<0.29±0.09	6.5±1.6
4449	<0.35±0.30	6.8±2.0	<0.25±0.05	2.5±1.9	1600±100	0.85±0.30	6.4±2.5
4569	0.00	...	0.00	...	...	0.00	...
4720	0.07±0.03	8.5±0.9	0.39±0.07	2.9±1.9	1600±100	0.13±0.02	9.0±1.6
4724	0.06±0.03	9.0±1.0	0.36±0.06	3.4±1.6	2380±240	0.15±0.02	9.0±1.4
4728	0.18±0.05	7.5±0.8	0.35±0.05	5.8±1.4	1810±180	0.06±0.03	5.4±2.0
4732	0.22±0.06	9.0±0.7	0.22±0.03	5.2±1.3	1890±190	0.02±0.01	3.9±1.7
4736	0.05±0.02	6.4±0.7	0.37±0.05	4.2±1.4	1700±100	0.00	...
4741	0.36±0.08	7.8±0.6	0.58±0.06	4.1±1.1	2090±200	<0.02±0.01	5.9±1.5
4747	0.54±0.10	7.5±0.6	0.60±0.06	3.3±1.2	2220±220	<0.10±0.03	8.6±1.5
4749	0.42±0.12	7.4±0.9	0.35±0.06	4.2±1.7	2810±280	<0.02±0.01	9.0±2.2
4754	0.35±0.06	7.5±0.6	0.55±0.09	4.1±1.2	1960±200	0.00	...
4760	0.41±0.08	6.8±0.6	0.56±0.10	4.0±1.3	1930±190	0.04±0.02	9.0±1.5
4764	0.37±0.07	7.1±0.6	0.62±0.11	3.9±1.2	2080±200	0.08±0.03	8.3±1.5
4781	0.53±0.12	3.5±0.8	0.50±0.06	2.5±1.3	2970±300	0.25±0.05	8.3±1.9
4783	0.26±0.07	6.8±0.9	0.57±0.15	2.5±1.8	2800±280	0.13±0.03	5.7±2.2
4785	0.38±0.10	7.2±0.8	0.53±0.07	2.5±1.4	2410±240	0.20±0.04	6.5±2.0
4789	0.30±0.09	7.7±1.0	0.40±0.1	4.0±2.0	2930±290	0.18±0.04	5.4±2.5
4792	0.29±0.06	8.0±0.7	0.49±0.10	4.0±1.3	2500±250	0.09±0.03	8.6±1.7
4802	0.08±0.03	5.8±0.9	0.18±0.03	6.6±1.3	2350±230	0.00	...
4813	0.25±0.09	7.9±1.2	0.44±0.08	4.6±1.8	3000±300	0.00	...
5020	0.39±0.08	7.0±0.7	1.08±0.11	3.6±0.8	2260±220	0.34±0.05	8.9±1.4
5026	0.51±0.10	6.8±0.7	0.88±0.09	3.3±0.9	2280±230	0.22±0.03	8.6±1.5
5029	0.48±0.10	5.1±0.7	1.05±0.10	2.5±0.8	2390±240	0.31±0.05	7.5±1.6
5077	0.60±0.09	4.2±0.6	0.77±0.06	3.1±0.6	2500±250	0.49±0.06	8.4±1.2
5078	0.62±0.12	5.9±0.7	0.93±0.09	3.1±0.8	2300±230	0.61±0.09	8.5±1.5
5280	0.10±0.02	6.6±0.5	<0.50±0.07	4.2±1.2	1600±150	0.73±0.08	8.4±1.1
5331	0.22±0.03	7.1±0.5	0.82±0.06	0.5±1.3	3000±300	0.41±0.05	4.7±2.4
5410	0.17±0.03	8.0±0.5	<0.22±0.04	1.5±1.5	2850±280	0.38±0.05	6.2±1.2
5413	0.02±0.01	8.6±0.6	<0.27±0.05	6.8±1.5	1600±100	<0.18±0.07	8.4±1.9
5417	0.30±0.06	6.6±0.5	0.43±0.04	4.8±0.9	1600±100	0.24±0.04	7.7±1.2
5420	0.35±0.08	7.2±0.6	0.31±0.03	4.1±1.0	1600±100	0.23±0.04	9.8±1.3
5471	<0.26±0.12	6.5±1.1	<0.38±0.16	5.8±3.2	1600±300	<0.25±0.18	9.6±2.5
5472	0.00	...	1.22±0.40	4.0±2.0	1600±250	1.28±0.19	8.7±2.0
5473	<0.41±0.15	6.1±0.6	0.66±0.10	3.4±1.1	2470±250	0.99±0.16	6.5±1.4
5638	0.47±0.09	8.2±0.6	0.94±0.10	2.8±1.0	3000±300	0.46±0.07	7.3±1.3
5643	0.38±0.08	6.9±0.6	0.68±0.06	1.8±0.8	3000±300	0.42±0.06	8.7±1.2
5646	0.30±0.07	7.8±0.7	0.65±0.07	1.5±1.0	3000±300	0.20±0.04	9.0±1.4
5650	0.40±0.10	7.0±0.8	0.76±0.08	0.9±1.0	3000±300	0.37±0.06	8.1±1.4
5654	0.32±0.08	8.5±0.8	0.51±0.06	1.5±1.0	3000±300	0.22±0.04	6.6±1.5
5658	0.32±0.07	7.3±0.7	0.57±0.06	1.6±0.9	3000±300	0.44±0.07	6.1±1.3

C IV red wing into the L2 and L'2 blend at low states. One would then expect the total intensity in the blend to be anticorrelated with L_0(C IV–B). However, the two variables are independent at the 99.9% confidence level. Moreover, I(L2 + L'2) is essentially the same (7.9 ± 4.5) when L_0(C IV–B) < 1535 Å (23 epochs) as when L_0(C IV–B) > 1545 Å (10.6 ± 6.1, 20 epochs).

Finally, in Figure 6*b* we plot the same diagram as in Figure 6*a*, but only for those data points which correspond to the well-sampled decay of 1983 October–November, together with the best-fit regression line corresponding to the whole data set. The sense of time is indicated with arrows connecting contiguous epochs. This clearly shows the gradual blueshifting of the C IV–B feature as it fades.

We therefore conclude that the L_0/I_0 correlation is a genuine property of the broad C IV λ1550 line. It strongly

TABLE 7

BEST-FIT PARAMETERS FOR THE N IV] λ1485, He II] λ1640, AND O III] λ1663 EMISSION LINES

J.D.	NIV]λ1485		HeIIλ1640	OIII]λ1663	
	Io	Lo-1480	Io	Io	Lo-1500
	(erg/cm²/s/A)	(A)	(erg/cm²/s/A)		(A)
3568	0.70±0.08	7.1±1.2	1.29±0.10	0.61±0.12	70.3±3.5
3615	0.89±0.10	3.0±1.0	1.33±0.11	0.61±0.12	68.0±2.0
3676	0.91±0.10	6.0±1.0	1.30±0.10	0.58±0.10	65.9±2.0
3714	0.93±0.10	4.8±1.0	1.26±0.10	0.44±0.09	61.2±3.0
3722	1.18±0.13	4.4±1.0	1.53±0.12	0.79±0.16	62.4±3.0
3801	1.19±0.13	5.9±1.0	1.10±0.09	0.46±0.10	60.4±2.0
3813	0.57±0.10	1.9±1.2	1.43±0.15	0.57±0.13	66.6±3.0
3851	0.66±0.07	4.4±1.0	1.28±0.10	0.60±0.12	62.1±2.0
3895	0.54±0.06	5.0±0.6	1.36±0.10	0.57±0.09	62.7±1.0
3996	0.96±0.11	3.8±0.6	1.45±0.10	0.53±0.08	61.2±1.0
3998	1.08±0.22	5.7±1.1	1.43±0.15	0.85±0.20	60.0±1.5
4012	0.96±0.11	4.2±0.6	1.39±0.10	0.50±0.08	59.9±1.0
4014	0.92±0.10	4.1±0.6	1.64±0.11	0.47±0.07	61.2±1.0
4016	1.00±0.11	6.1±0.6	1.46±0.10	0.58±0.09	61.4±1.0
4018	0.91±0.10	4.5±0.6	1.55±0.11	0.50±0.08	61.3±1.0
4025	0.93±0.17	3.3±1.0	1.40±0.17	0.30±0.08	69.7±1.8
4025	1.15±0.13	5.0±0.6	1.43±0.10	0.50±0.08	61.1±1.0
4093	0.72±0.08	5.7±0.6	1.32±0.09	0.45±0.07	62.5±1.0
4215	0.55±0.06	5.8±0.6	1.32±0.09	0.45±0.07	63.1±1.0
4220	0.70±0.08	4.4±0.6	1.02±0.07	0.24±0.05	64.7±1.0
4220	0.73±0.08	5.6±0.6	1.08±0.07	0.24±0.05	64.5±1.0
4239	0.62±0.06	3.5±0.6	1.32±0.08	0.50±0.07	61.5±1.0
4299	0.78±0.07	4.2±0.5	1.32±0.07	0.50±0.05	61.5±0.8
4302	0.85±0.09	3.1±0.6	1.07±0.07	0.57±0.07	60.5±1.0
4304	0.86±0.08	2.9±0.5	1.20±0.07	0.56±0.07	60.5±0.9
4342	0.71±0.10	4.5±0.8	1.47±0.13	0.56±0.11	61.8±1.3
4350	0.84±0.09	4.1±0.6	1.43±0.10	0.50±0.08	62.7±1.0
4374	0.86±0.10	5.2±0.6	0.99±0.10	0.35±0.10	58.8±1.5
4378	0.97±0.07	4.1±0.6	1.40±0.10	0.50±0.06	60.6±1.0
4449	0.97±0.16	5.0±1.0	1.40±0.10	0.50±0.13	60.1±1.7
4569	0.47±0.10	7.0±1.2	0.98±0.13	0.19±0.16	65.4±1.8
4720	0.58±0.08	6.9±0.8	1.33±0.16	0.34±0.09	62.6±1.5
4724	0.44±0.06	6.4±0.7	1.28±0.14	0.49±0.12	61.7±1.4
4728	0.60±0.07	4.5±0.7	1.23±0.12	0.44±0.10	62.8±1.3
4732	0.50±0.05	5.4±0.6	1.21±0.11	0.38±0.07	62.7±1.1
4736	0.49±0.05	5.0±0.6	1.17±0.11	0.40±0.08	61.8±1.2
4741	0.55±0.05	4.7±0.5	1.35±0.10	0.39±0.06	63.3±1.0
4747	0.55±0.05	4.1±0.5	1.19±0.09	0.44±0.07	62.7±1.0
4749	0.65±0.09	4.2±0.8	1.40±0.17	0.37±0.09	63.1±1.5
4754	0.54±0.05	4.9±0.5	1.35±0.09	0.42±0.06	62.2±0.9
4760	0.57±0.05	4.7±0.5	1.28±0.09	0.43±0.06	62.6±1.0
4764	0.66±0.06	4.6±0.5	1.24±0.09	0.42±0.06	62.4±0.9
4781	0.70±0.08	6.3±0.6	1.24±0.11	0.52±0.09	62.7±1.1
4783	0.59±0.08	5.2±0.7	1.27±0.13	0.57±0.12	63.5±1.3
4785	0.52±0.06	5.6±0.7	1.22±0.12	0.37±0.07	62.8±1.2
4789	0.61±0.09	4.2±0.8	1.20±0.14	0.41±0.10	64.1±1.5
4792	0.55±0.06	4.7±0.6	1.39±0.11	0.47±0.08	63.4±1.0
4802	0.53±0.07	5.1±0.8	1.21±0.10	0.45±0.08	62.8±1.3
4813	0.34±0.07	6.4±1.0	1.12±0.14	0.47±0.12	61.9±1.8
5020	0.50±0.05	4.7±0.5	1.04±0.07	0.45±0.07	61.1±1.0
5026	0.48±0.05	3.5±0.5	1.02±0.07	0.43±0.06	62.7±1.0
5029	0.64±0.07	4.3±0.5	0.83±0.07	0.46±0.07	62.8±1.0
5077	0.77±0.07	4.6±0.4	1.04±0.06	0.27±0.05	57.8±0.6
5078	0.73±0.08	6.3±0.5	1.17±0.08	0.39±0.06	59.3±1.8
5280	0.58±0.05	5.6±0.4	1.49±0.08	0.63±0.07	62.0±0.7
5331	0.67±0.06	3.8±0.4	1.23±0.07	0.48±0.05	63.4±0.8
5410	0.72±0.07	4.8±0.5	1.46±0.09	0.58±0.08	63.1±0.9
5413	0.76±0.08	5.2±0.5	1.46±0.10	0.58±0.08	62.5±0.9
5417	0.68±0.07	5.3±0.4	1.49±0.09	0.53±0.07	61.8±0.9
5420	0.65±0.07	5.6±0.5	1.38±0.10	0.59±0.09	61.9±1.0
5471	0.65±0.15	6.0±1.0	1.38±0.18	0.59±0.20	68.0±3.0
5472	0.65±0.11	1.5±0.8	1.38±0.13	0.99±0.20	62.1±2.0
5473	0.94±0.11	6.1±0.5	1.70±0.13	0.59±0.11	61.9±1.1
5638	0.57±0.06	5.4±0.5	1.37±0.10	0.53±0.08	62.9±1.0
5643	0.59±0.06	5.8±0.5	1.28±0.08	0.54±0.08	61.0±0.9
5646	0.50±0.06	4.9±0.5	1.36±0.10	0.53±0.08	61.9±1.1
5650	0.58±0.07	5.1±0.6	1.31±0.10	0.48±0.08	62.5±1.1
5654	0.67±0.09	4.9±0.7	1.36±0.11	0.43±0.08	63.0±1.2
5658	0.57±0.07	4.5±0.6	1.35±0.10	0.44±0.07	62.4±1.0

suggests the existence of *radial* motions of the gas plus some kind of obscuration. A more detailed interpretation is proposed in § IV.

c) *The Broad* He II *Emission Component*

The broad helium feature is detected only 59% of the time. It seems to be present only when the continuum is above a threshold of $\sim 0.6 \times 10^{-13}$ ergs cm^{-2} s^{-1} Å^{-1}. This is, however, not a sufficient condition, since, for instance, on 1979 May 3–4, early in the outburst, the He II broad component is not detected, whereas the continuum intensity is already $\sim 1 \times 10^{-13}$ ergs cm^{-2} s^{-1} Å^{-1}. When He II–B is present, its fractional range of variation is comparable to that of the continuum or the broad C IV line (factor of ~ 7). I_0(He II–B) is correlated with the continuum flux at $\gg 99.9\%$ confidence level ($r = 0.88$ for 67 degrees of freedom). Excluding those epochs when the He II–B line is not detected yields a best-fit regression line ($r = 0.58$; $\chi^2 = 6.3$) which, as for C IV–B, goes through the

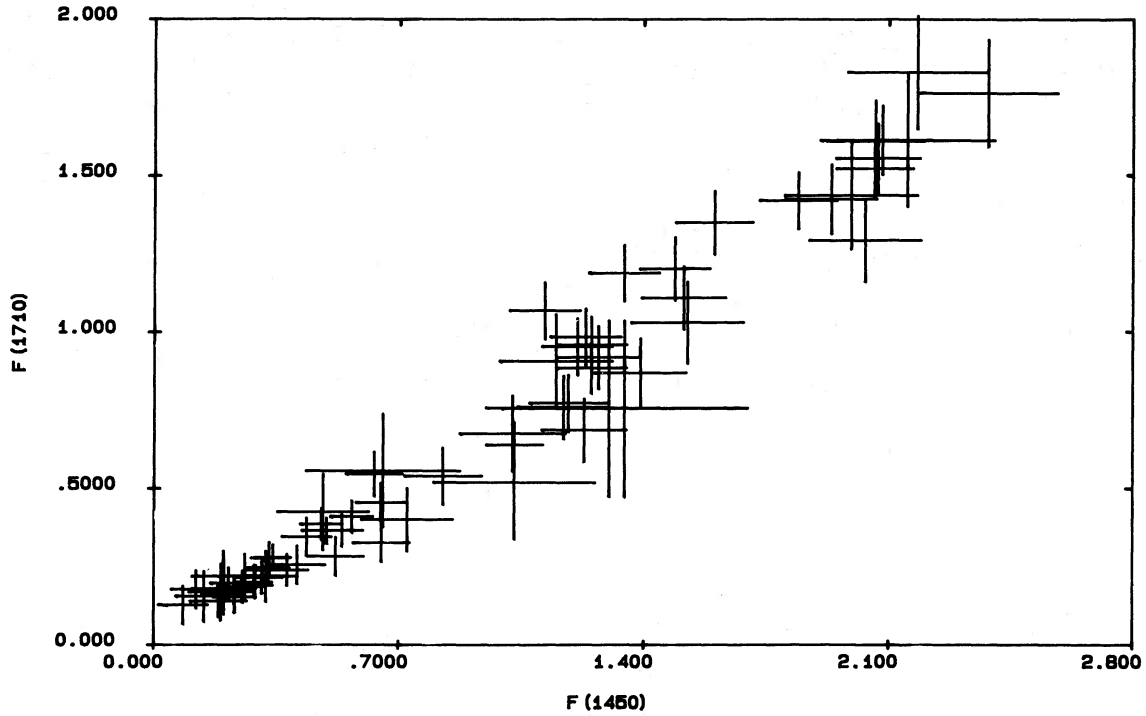

FIG. 3.—Continuum intensity at 1710 Å vs. that at 1450 Å. As in most figs., data points are presented with their associated error bars. Strong correlation between the two intensities and fact that regression line passes through origin shows that spectral index of continuum in this wavelength region remains constant when its intensity varies.

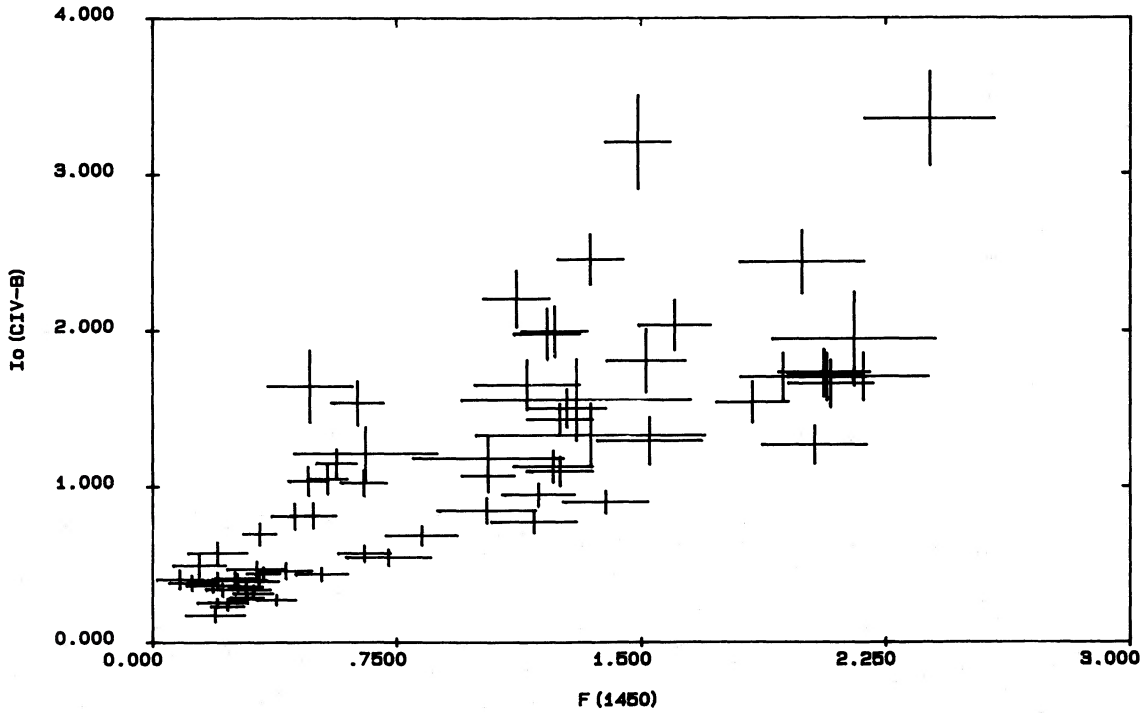

FIG. 4.—Peak intensity of broad (14,600 km s^{-1} FWHM) C IV λ1550 emission component vs. intensity of continuum at 1450 Å. This shows good (but imperfect) correlation. Our interpretation is that broad C IV λ1550 lines arises in a gas which is photoionized and lies sufficiently close to continuum source that light travel time is comparable to time scale of variation.

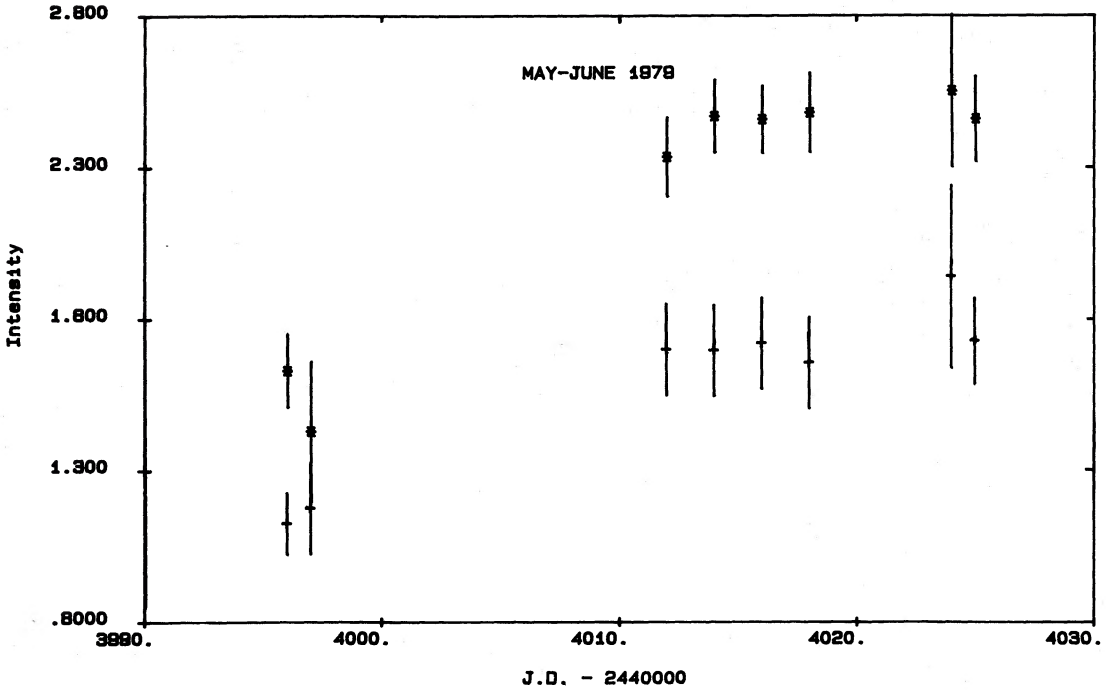

FIG. 5*a*

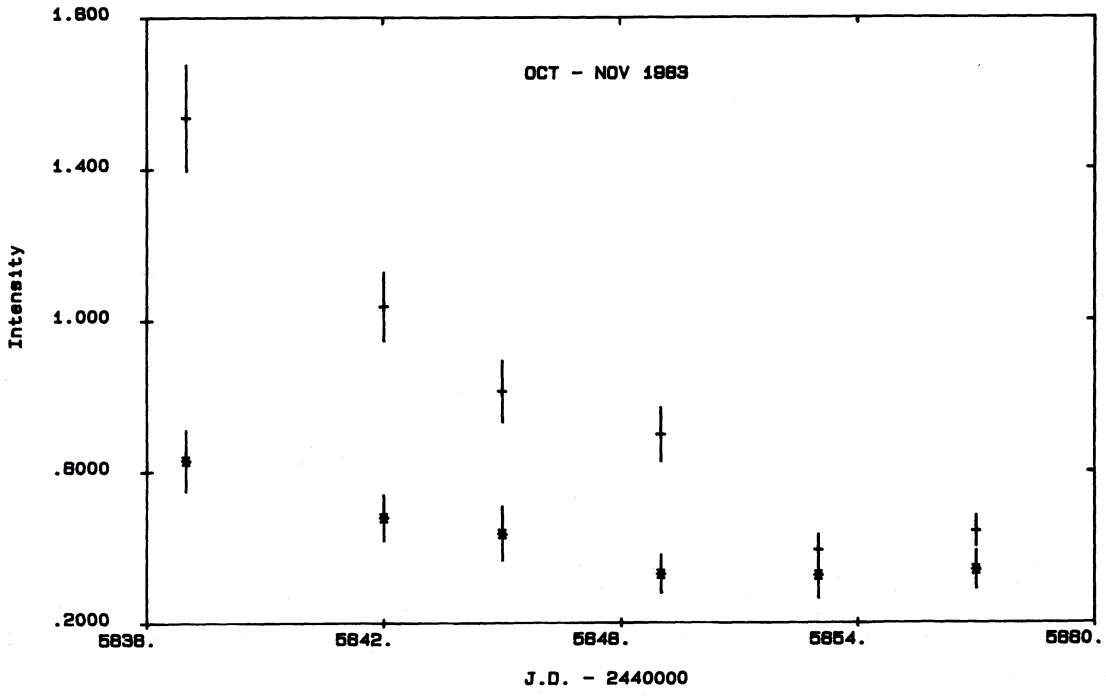

FIG. 5*b*

FIG. 5.—Intensities of C IV–B, broad C IV λ1550 component (*cross*) and continuum (*asterisk*) at 1450 Å are shown as function of time (Julian Date −2,440,000.5) for different episodes of rapid variability: (*a*) 1979 May–June outburst; (*b*) 1983 October–November decay; (*c*) 1981 April–July fluctuations. For sake of clarity, continuum light curves have been artificially shifted upward by 0.4×10^{-13} ergs cm^{-2} s^{-1} Å^{-1} in (*a*) and (*c*). Solid line of (*d*) represents cross-correlation function (CCF) of C IV–B light curve with that of continuum for entire 1978–1983 episode. Auto-correlation function (ACF) of C IV–B light curve (*broken line*) is also shown for reference. As expected, ACF peaks at 0, while CCF has its maximum at −9 days, which, as explained in text, probably represents upper limit to actual lag in variations of C IV–B component over those of continuum. The well-sampled episodes illustrated in (*a*)–(*c*) suggest a delay of ~5 days for the response of I_0(C IV–B).

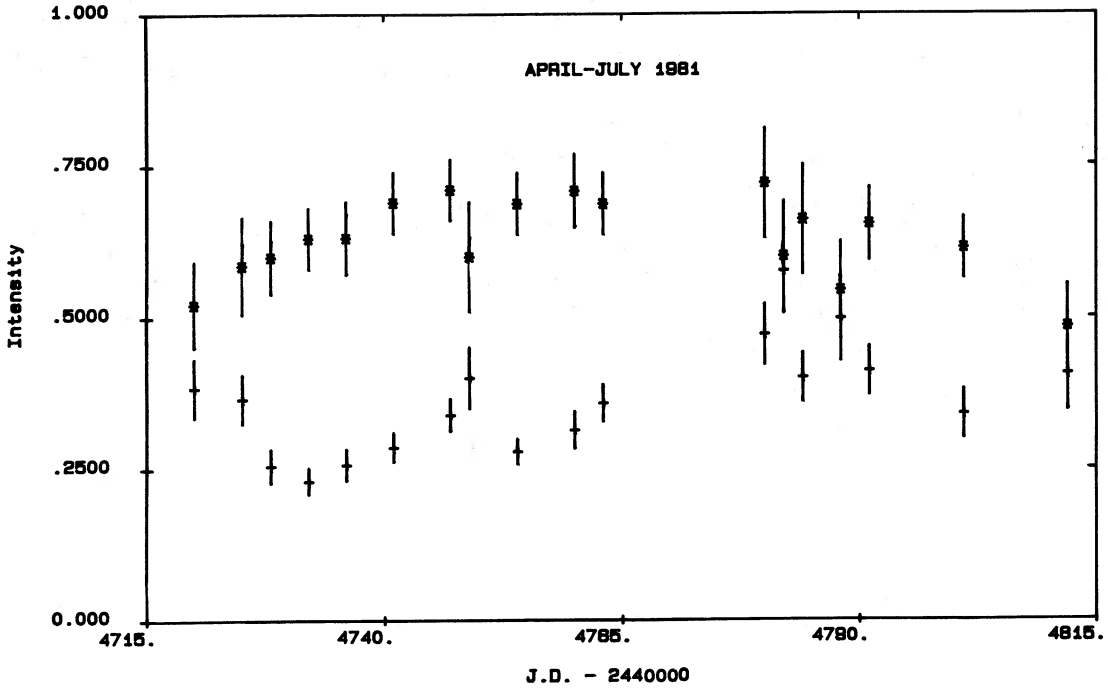

FIG. 5c

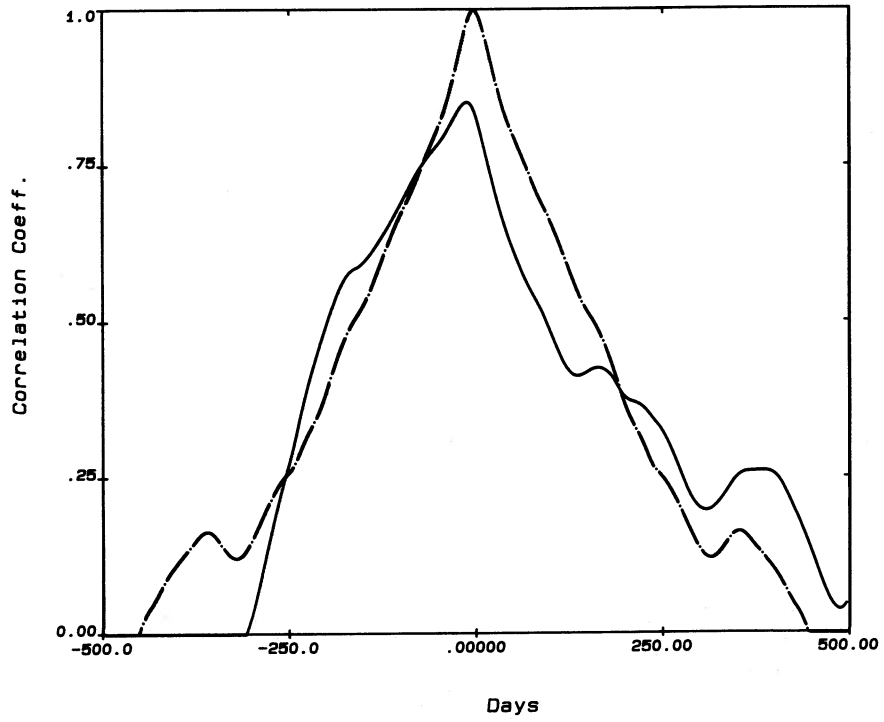

FIG. 5d

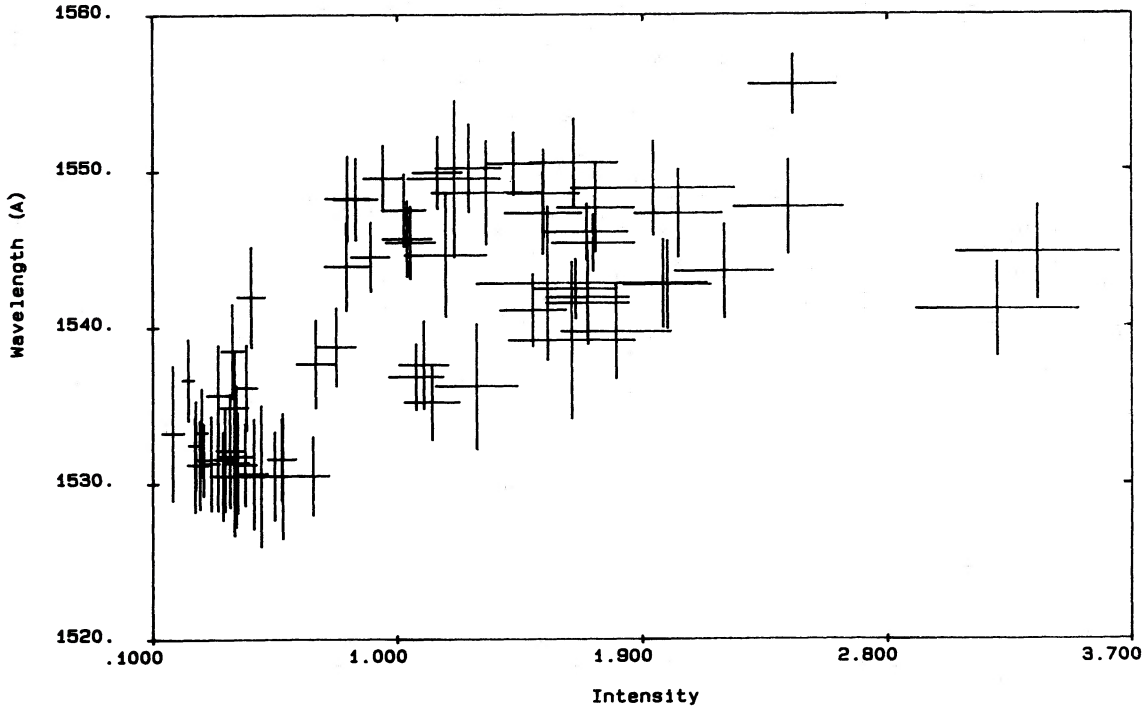

FIG. 6a

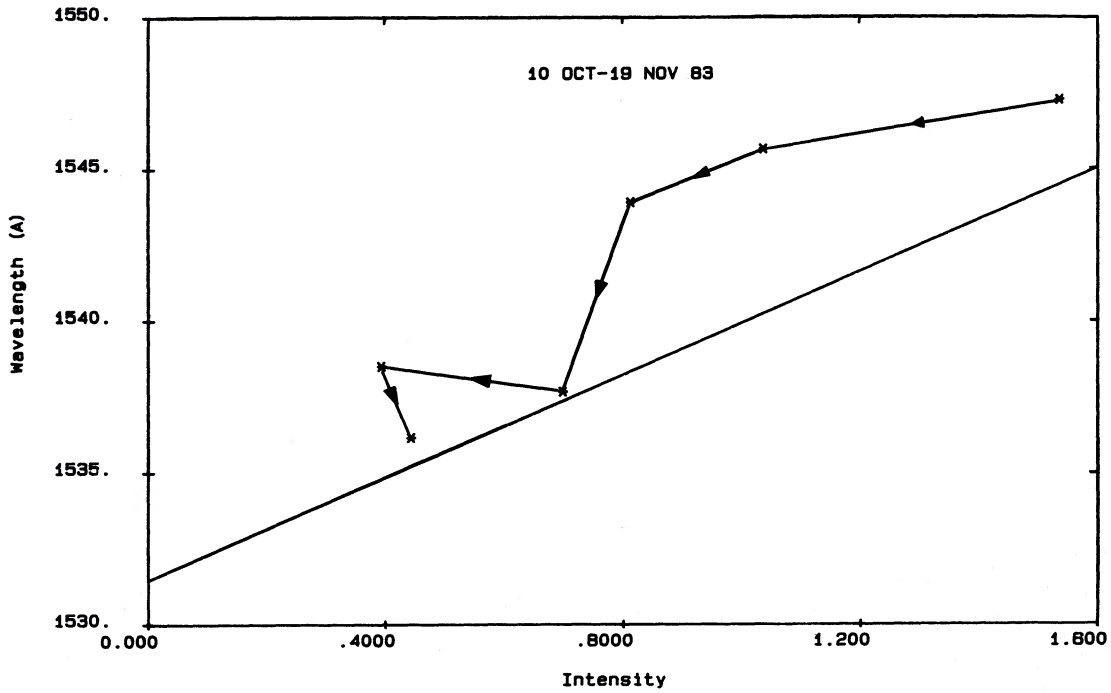

FIG. 6b

FIG. 6.—Wavelength L_0 (in velocity frame of NGC 4151) of broad C IV λ1550 emission component vs. its intensity I_0. In (*a*), all data points are plotted together with their error bars. This clearly shows that L_0 and I_0 are correlated. In (*b*), we have represented only those points which correspond to the well-sampled decay of 1983 October–November. Error bars are omitted for clarity, and sense of time is indicated by arrows connecting contiguous epochs. The best-fit regression line corresponding to entire sample (see text) is also drawn for comparison. (*b*) Data confirm that broad C IV feature gradually shifts toward negative velocities as its intensity decreases; this shift is interpreted as evidence for outflowing gas within innermost 5 lt-day of nucleus.

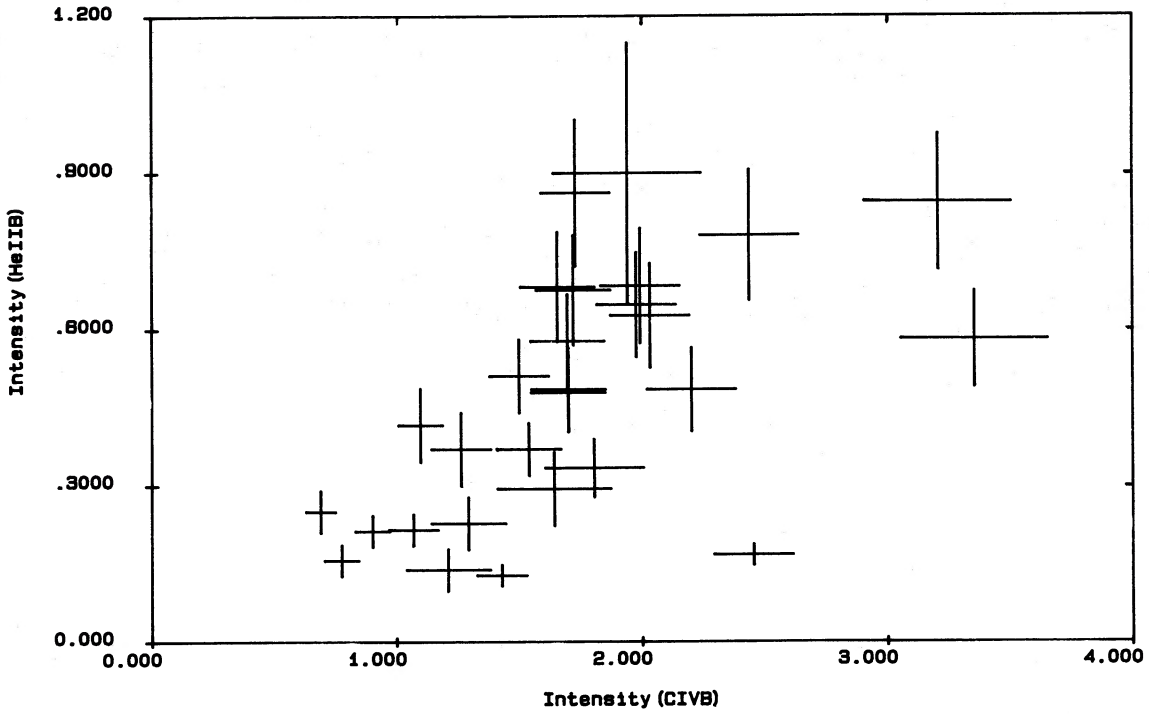

FIG. 7.—Intensity of broad He II λ1640 line vs. that of broad C IV component. Intensities of the two features are clearly (though imperfectly) correlated, which suggests that broad C IV and He II lines originate from overlapping subregions of BLR.

origin, but with a much shallower slope (0.23). Figure 7 displays I_0(He II–B) versus I_0(C IV–B). As expected, the two variables are also correlated at the 99.8% level of confidence. A linear fit ($r = 0.58$, $\chi^2 = 7.9$) yields

$$I_0(\text{He II–B}) = (0.22 \pm 0.01) I_0(\text{C IV–B}) + (0.00 \pm 0.01) .$$

It is therefore concluded that the gas responsible for the broad He II emission shares some common properties with the broad C IV emitting material. Though the two emitting regions probably overlap, the smaller FWHM suggests that the bulk of the He II–B emitting material is located somewhat further out than is the broad C IV gas.

During the 1979 May–June outburst, the onset of the broad He II line took, at most, 17 days (May 3–19). Note that on May 19, He II–B has already acquired its average intensity. On the other hand, the plateau which is seen in the continuum (and C IV–B) light curve after May 19 is not reflected in the light curve of I_0(He II–B) up to June 1. Both the onset time and the lag constrain the mean radius of the broad helium line emitting region to be in the range 13 to 17 lt-day, somewhat larger than the dimensions of the C IV–B emitting shell.

The broad helium feature is only 5 times weaker than the C IV–B line on the average and should therefore be easily detectable most of the time, except perhaps when I_0(C IV–B) drops below 0.4×10^{-13} ergs cm^{-2} s^{-1} Å^{-1}. Its complete absence at low and intermediate states—in particular when C IV–B is still strong—is therefore intriguing. The He^{2+} and C^{3+} ions having very similar ionization potentials, the physical conditions of the C IV–B emitting gas must be rather peculiar. This point is discussed further in § IV*b*.

In contrast with the broad C IV component, the wavelength of the broad He II line is not correlated ($r = -0.19$) with its intensity. On a few occasions, the He II line is significantly displaced to the red with respect to its laboratory wavelength (up to 15 Å). This suggests that the He II line is sometimes blended with a much weaker broad O III] λ1663 component.

d) The C IV *λ1549.5 Emission Core*

The peak intensity of the emission core of C IV λ1550, I_0(C IV–B), is *not* correlated with the continuum flux, F(1450) ($r = 0.04$). A comparison of the two light curves confirms that the two quantities are indeed independent. For instance, during the 1979 May–June outburst, the increase of I_0(C IV–C) is only marginal (2.35 σ), whereas that of the continuum is highly significant (4.5 σ).

The peak intensity of the C IV emission core averaged over the entire 1978–1983 episode is $(9.1 \pm 0.8) \times 10^{-13}$ ergs cm^{-2} s^{-1} Å^{-1}. The variations of I_0(C IV–C) appear to be real, however, since, for instance, on 1979 January 21 and 1982 November 16 it is, respectively, 5.1 and 11.0 σ above and below this mean value. Note that the continuum intensity is approximately the same at the two epochs.

The width of the C IV emission core, FWHM(C IV–C), is correlated, however, with the continuum intensity at the 99.9% confidence level (Fig. 8). A linear fit ($r = 0.85$ $\chi^2 = 6.8$) yields

$$\text{FWHM(C IV–C)} = (1500 \pm 25) F(1450) + (2060 \pm 20) \text{ (km s}^{-1}\text{)}$$

This relationship suggests that the C IV core contains both a constant 2060 km s^{-1} FWHM component as well as a variable and higher velocity line. The variable contribution being proportional to F(1450), it presumably represents emission from a gas which is close to the continuum source and responds to changes in the photoionization rate. The constant component, on the other hand, contains the residual C IV flux which would remain after the continuum source is turned off.

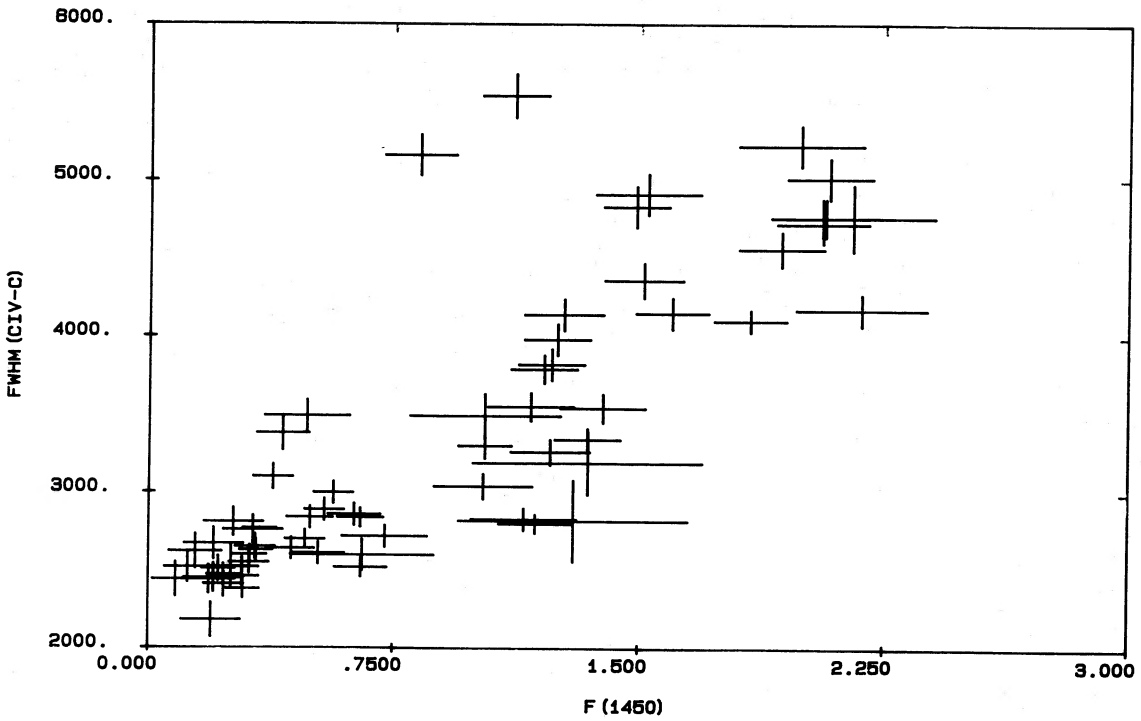

FIG. 8.—Full width at half-maximum (FWHM, km s^{-1}) of C IV λ1550 emission core vs. intensity of continuum at 1450 Å. The two quantities are clearly correlated. Best-fit regression line (not shown) does not go through origin. This suggests that C IV λ1550 emission core contains both a rapidly variable component as well as more or less stable contribution from a region whose velocity dispersion is $\sim$1600 km s^{-1}. Variable line is found to originate in a region whose "radius" is $\sim$25 lt-days, whereas constant component comes from larger ILR which also emits He II λ1640 core, O III] λ1663, and bulk of C III] λ1908 and N IV] λ1485 lines (see text).

Therefore, we interpret it as emission from an extended region which lies too far away from the continuum source to be sensitive to the variations of the photoionization rate. Taking into account the 1548.2–1550.8 Å doublet separation, the intrinsic width of this component is 1560 km s^{-1}, interestingly close to that of the other slowly variable or nonvariable emission lines, i.e., the He II λ1640 core, the C III] λ1908 core, the N IV] λ1485, and the O III] λ1663 (see § III*g*). This suggests that these five features originate in the outskirts of the BLR, where the velocity dispersion of the gas is 1600 km s^{-1}. This well-identified subregion corresponds to the BLR3 of Paper III. However, since BLR1 and BLR2 are no longer uniquely defined (see § II*a*), this terminology was dropped and BLR3 was renamed ILR, for intermediate-width line region.

The velocity dispersion of the variable C IV core emitting gas is at least 5500 km s^{-1}, the highest value of FWHM (C IV–C) recorded so far. This is only a lower limit, however, since the core of the C IV line includes a constant ILR (and NLR) contribution which is narrower and sharpens the overall profile even though we cannot resolve it.

A cross-correlation analysis of the FWHM (C IV–C) and F(1450) light curves does not yield convincing evidence for time delays, probably because any such lag is not properly sampled by the present data. The only marginally significant result is obtained for the well covered 1981 episode and suggests a delay of $\sim$20 days. Upper limits R_{max} to the mean radius of the emitting region are also provided by the two-folding time scales of the C IV core intensity as measured during the 1978 October 19–31 (decay) and 1979 May 3–25 (outburst) rapid variations. After subtraction of a constant 2060 km s^{-1} FWHM ILR component, these two events yield R_{max} = 26 and 28 days respectively, consistent with the above value. We therefore assign a tentative value of 25 lt-days to the radius of the C IV core emitting region.

The mean wavelength of the C IV core, averaged over all epochs of observation, is 1547.5 $\pm$ 1.1, which implies that the emitting material has a bulk velocity in the range from -130 to -190 km s^{-1}, depending on the C IV $\lambda\lambda$1548.2–1550.8 doublet intensity ratio. This wavelength is, however, variable; the largest difference (1978 October 19–1982 April 17), 5.9 Å, is significant at the 10 σ level. These variations do not correlate with those of the continuum, nor with the peak intensity of the core itself. However, L_0(C IV–C) is correlated with FWHM(C IV–C) (r = 0.67), when the line width increases, the additional energy tends to appear more in the red wing than in the blue part of the profile. Such a trend is reminiscent of the correlation found earlier between the wavelength and the intensity of the broad C IV component.

e) The C IV *Absorption Line*

The strength of the C IV absorption line cannot be reliably measured when the source is in a faint state and the emission-line core is narrow (FWHM < 3000 km s^{-1}). In such cases, the absorption being displaced toward negative velocities, the blue part of the emission profile is missing and the local continuum (i.e., what is absorbed) is no longer well-defined (see for instance the spectrum of Fig. 2*b*). Moreover, the number of dominant free parameters and resolution elements in the C IV core spectral range become comparable. As a result, the fit becomes unstable (the χ^2 "wells" are no longer sharp and deep) and seems to overestimate the strength of the absorption

feature. This affects also the intensity of the emission core, though the relative error is much smaller than for the absorption line. Therefore, for all epochs when FWHM(C IV–C) is less than 3000 km s^{-1}, the optical depth T_0 and equivalent width EW of C IV–A in Table 5 have been flagged as upper limits.

The remaining values of EW(C IV–A) are, on the average, a factor of 2 higher than those of Paper IV. This is no surprise, since, in Paper IV, a local continuum joining the apparent emission maxima on either side of the absorption was used to compute EW(C IV–A). Therefore, the values quoted in Paper IV are only lower limits to the actual equivalent widths, whereas those of Table 5 are probably more realistic.

The equivalent width of the C IV absorption line is *not* significantly correlated with the intensity of the continuum (confidence level is only 95%). Altogether, the variations of EW(C IV–A) are only marginal. The largest change (1978 August 2–1979 December 12) is only significant at the 3.3 σ confidence level. Note that the continuum intensity is approximately the same at the two epochs. The present data certainly exclude a strong positive correlation of EW(C IV) with $F(1450)$ such as was found in Paper IV for, e.g., EW(N V λ1240). Tests have been run to force such a correlation for a limited subset of epochs at low and high states. They invariably yield unacceptable fits which fail both the χ^2 test (e.g., 5.3 and 5.6 for the 1981 April 21 low and 1979 June 1 high states, respectively) and the Kolmogorov test (at the 1% level). The present result suggests that a constant absorption component is hidden in the C IV profile.

The wavelength of the C IV absorption line is not significantly correlated with the intensity of the continuum (confidence level is 91%). The mean value of L_0(C IV–A) is 1545.3 ± 1.3 Å, which corresponds to a velocity of -720 ± 250 km s^{-1}, in good agreement with the results of Paper IV for the N V λ1240, C II λ1335, and Si IV λ1400 absorption features (-820 ± 100 km s^{-1}; Paper IV).

Veron, Veron-Cetty, and Tarenghi (1985) concluded that the equivalent width of the absorption lines in NGC 4151 do not vary. This clearly conflicts with the results of Paper IV where it was found that the equivalent widths of lines of highly excited ions (e.g., N V, Si IV, but *not* C IV) are *positively* correlated with the intensity of the continuum at a high level of significance, whereas those of "low" ions (in particular Al III and Si II) are *anticorrelated*. The case of C IV was inconclusive ($r = 0.24$ for 29 degrees of freedom, which means that the correlation was significant at the 80% level only). The disagreement stems from the fact that Veron and collaborators based their results on two lines only—C II λ1335 and C IV λ1550—whereas our conclusions were derived from the analysis of 14 different features. We agree with them on the absence of strong variations of the C IV equivalent width, though as explained above, this is only a weak statement given the large measurement uncertainty during the low states of NGC 4151. As far as the C II λ1335 line is concerned, their results are also roughly in agreement with ours simply because the excitation potential of this feature happens to lie in the transition regime where the equivalent width are neither correlated nor anticorrelated with the continuum intensity. However, we disagree with them when they extrapolate their results and state that the equivalent widths of the absorption lines as a whole do not vary. If Veron and coworkers had included in their study other absorption lines, more strongly variable or less difficult to measure—such as Si II λ1260, Al II λ1858, Si IV λ1400, or N V λ1240—their conclusions could not have been sustained.

f) *The Unidentified* L1, L2, *and* L′2 *Emission Lines*

For those epochs where the broad C IV λ1550 emission component is intense, and the L1, L2, and L′2 lines are not visually recognizable in the spectra, the intensities of these features have been flagged as upper limits in Table 6.

The integrated intensities of L1, L2, L′2 are *not* correlated with the continuum flux, $F(1450)$:

$$\text{L1}: r = 0.03\ (0.18)\,, \quad \chi^2 = 25.8\ (12.7);$$

$$\text{L2}: r = 0.02\ (0.40)\,, \quad \chi^2 = 7.1\ (8.0);$$

$$\text{L}'2: r = 0.53\ (0.58)\,, \quad \chi^2 = 7.5\ (7.5):$$

all χ^2 values are reduced. (The above values in parenthesis obtain when the upper limits of Table 6 are excluded from the regression analysis.) This is confirmed by a close comparison of the two light curves. For instance, in 1981, the continuum is extremely faint and hardly varies, while both the intensities of L1 and L2 increase by a factor of ~ 3.5 and are rather strong on the average. Conversely, in 1980 May, these lines are weak even though $F(1450)$ is intense. The upper limits of Table 6 are useful because they permit us to rule out the possibility that L1, L2, L′2 become strong when the nucleus is in a bright state (e.g., 1979 May–June).

We therefore confirm the result of Paper V: in contrast with the other ultraviolet emission lines, the variations of L1, L2, and L′2 are *not* linked to that of the continuum, and we reemphasize our conclusion that their intensity is *not* governed by photoionization. Clearly, the excitation mechanism of L1, L2, and L′2 must be distinct from that of the other emission lines. Based on the fact that (1) they do not lie at the wavelength of known strong features either in the laboratory or in astrophysical sources, and (2) they are relatively narrow, but (3) still vary quite rapidly, in Paper V we tentatively identified L1 and L2 (including L′2) as, respectively, a blueshifted and a redshifted C IV emission feature excited by the interaction of the two-sided radio jet (Johnston *et al.* 1982; Booler, Pedlar, and Davies 1982) with the BLR clouds. If the slight difference in velocity shift is interpreted in terms of relativistic transverse Doppler effect, it yields an inclination of 75° with respect to the line of sight (LOS) and a velocity of 28,500 km s^{-1} for the jet. While these values are somewhat uncertain and should be treated with caution, we shall see below that some independent piece of information definitely constrains the jet to lie close to the plane of the sky.

Figure 9 shows the integrated intensity of L1 versus that of L2 + L′2. The two quantities are correlated at the 99.9% confidence level ($r = 0.58$, $\chi^2 = 2.9$). Attempts to correlate L1 with either L2 or L′2 alone yield slightly worse results ($r = 0.50$, $\chi^2 = 3.3$). This suggests that the L2 and L′2 lines are a single entity, even though the global feature clearly shows a double peak on certain occasions. The two possibly originate from nearby obstacles along the path of the jet. The above correlation puts strong constraints on the distance of the obstacles to the origin of the jet as well as on the orientation of the jet with respect to the LOS. Indeed, if one interprets the variations of L1 and L2 + L′2 as being due to a rapid change in the amount of kinetic energy carried by the jet, then the two signals emitted by the obstacles must reach the observer almost simultaneously for the above correlation to hold.

Figures 10*a* and 10*b* display the integrated intensity of L1, I(L1), versus that of L2 + L′2, I(L2 + L′2), for two different episodes, namely 1981 April 26–July 27 and 1983 October 30–

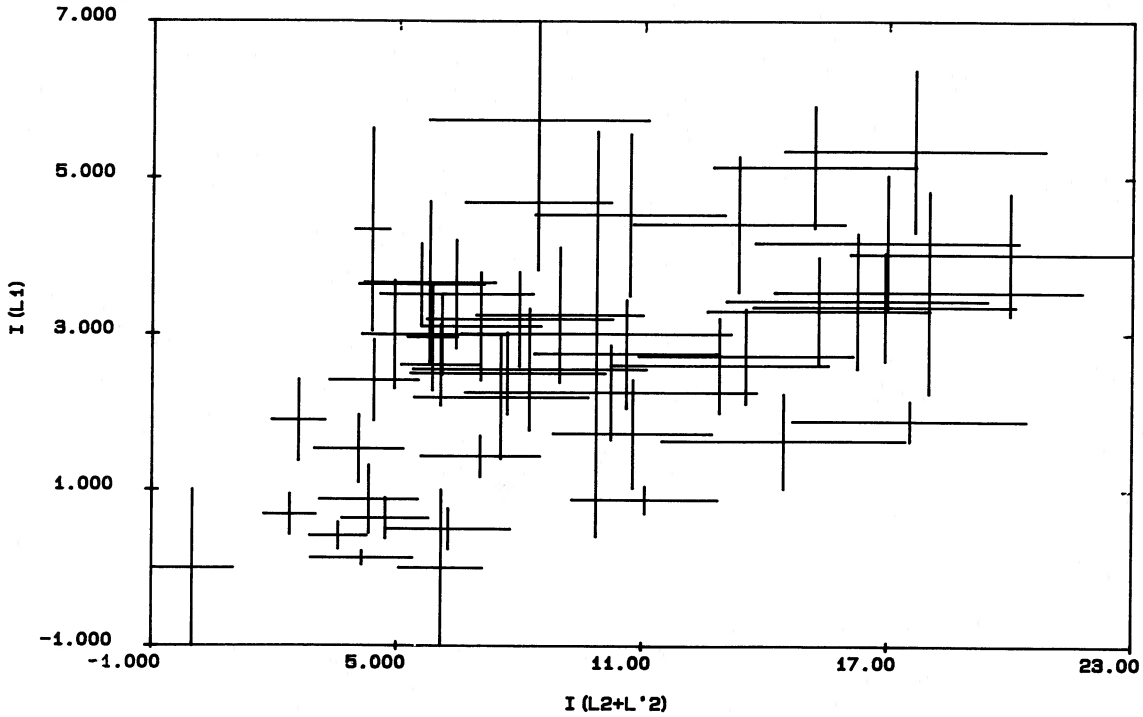

FIG. 9.—Integrated intensities of L1 λ1518 and L'2 λ1576 + L2 λ1594 blend plotted against each other. These are clearly correlated which shows that they must be excited by same mechanism. This mechanism is *not* photoionization, since neither of the two line intensities is significantly correlated with continuum flux. We interpret L1 and L2 + L'2 lines as Doppler-shifted C IV lines excited by two-sided radio jet (see text).

November 19. These episodes are most appropriate to determine time delays, because in both cases the light curves have been sampled at short intervals over a relatively long time span. Data points for consecutive epochs have been connected by arrows to indicate the direction of time. A regression analysis yields the following results:

$$1981: I(\mathrm{L1}) = (0.37 \pm 0.04)\ I(\mathrm{L2} + \mathrm{L'2}) + (0.00 \pm 0.04);$$
$$1983: I(\mathrm{L1}) = (0.16 \pm 0.02)\ I(\mathrm{L2} + \mathrm{L'2}) + (0.69 \pm 0.34)\,.$$

The first remark is that the significance of the correlation has drastically improved as compared to that found for the entire data set ($r = 0.71$, $\chi^2 = 2.1$, and $r = 0.90$, $\chi^2 = 0.1$ for 1981 and 1983, respectively). Second, the best-fit regression lines have significantly different slopes and zero points at the two epochs. This shows that the intensities of the two features are well correlated over a short time scale, but that their mean ratio can vary by large amounts from one episode to another. The later trend accounts for the weaker correlation found earlier for the entire data set.

It is not clear from Figure 10 whether L2 lags behind L1, or if the opposite situation applies. Both the 1981 and 1983 episodes suggest that if there is any delay, T_d, it is extremely small on the average. The 1983 October–November data are consistent with $T_d \approx 0$. In 1981, the situation is more complex: at the end of April to the beginning of May, L2 leads over L1 by $\sim$4 days; then, both lines remain in phase, except maybe in late June when it is now L1 which leads by at most 2 days. Attempts to cross-correlate the L1 and L2 light curves (all data after 1980) yield a broad maximum around $T_d = 0$. We therefore conclude that *on the average, there is no delay between the variations of* L1 *and* L2. Intuitively, one would expect the signal of L1 (near side of the nebula) to reach the observer first, whereas that of L2, which by definition is emitted from the far side, has a longer distance to travel and should therefore be received systematically later. The fact that this is not so provides an independent confirmation that the jet lies very close to the plane of the sky.

Let D_1 and D_2 be the distances, measured from the origin of the jet to the obstacles which emit the L_1 and L_2 lines, respectively. Taking 4 days as a conservative upper limit to T_d, and using the velocity and inclination of the jet found in Paper V, one finds

$$D_2 - D_1 < 1 \times 10^{+15}\ \mathrm{cm}\,,$$
$$D_2 + D_1 < 4 \times 10^{+16}\ \mathrm{cm}\,.$$

The first symmetry condition is imposed by the relatively slow velocity of the jet, whereas the second one sets a limit to the additional path which the light from L2 has to travel as compared to the distance which L1 must travel. Together, the two conditions constrain the obstacles to be within 2×10^{16} cm of the origin of the jet. Since the later presumably coincides with the location of the continuum source, this suggests that L1 and L2 originate within the same gas which produces the broad C IV λ1550 emission line. An interesting consequence is that the bulk velocity of the jet is subrelativistic at only a few light-days from its origin.

g) The N IV *λ1485,* He II *λ1640 Core, and* O III] *λ1663 Emission Lines*

The light curves of N IV] λ1485. He II λ1640 core, and O III] λ1663 are displayed in Figure 11.

The N IV] line shows significant variations with a maximum fractional range, $D(I) = (I_{\max} - I_{\min})/I_{\min} = 2.5 \pm 1.1$, at the

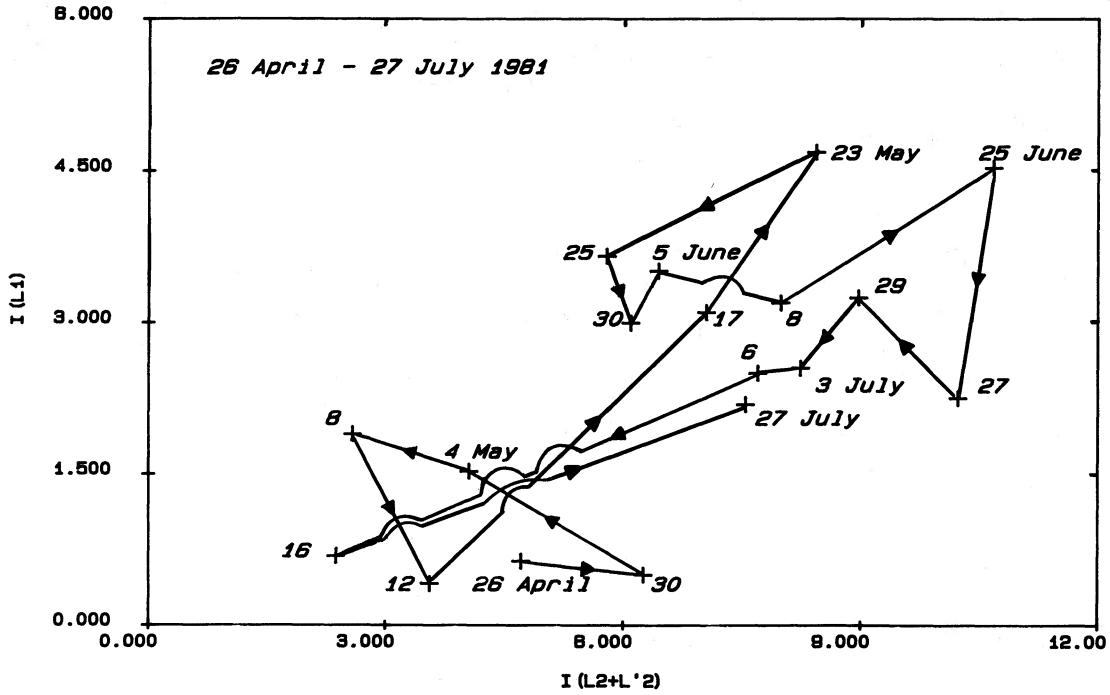

FIG. 10*a*

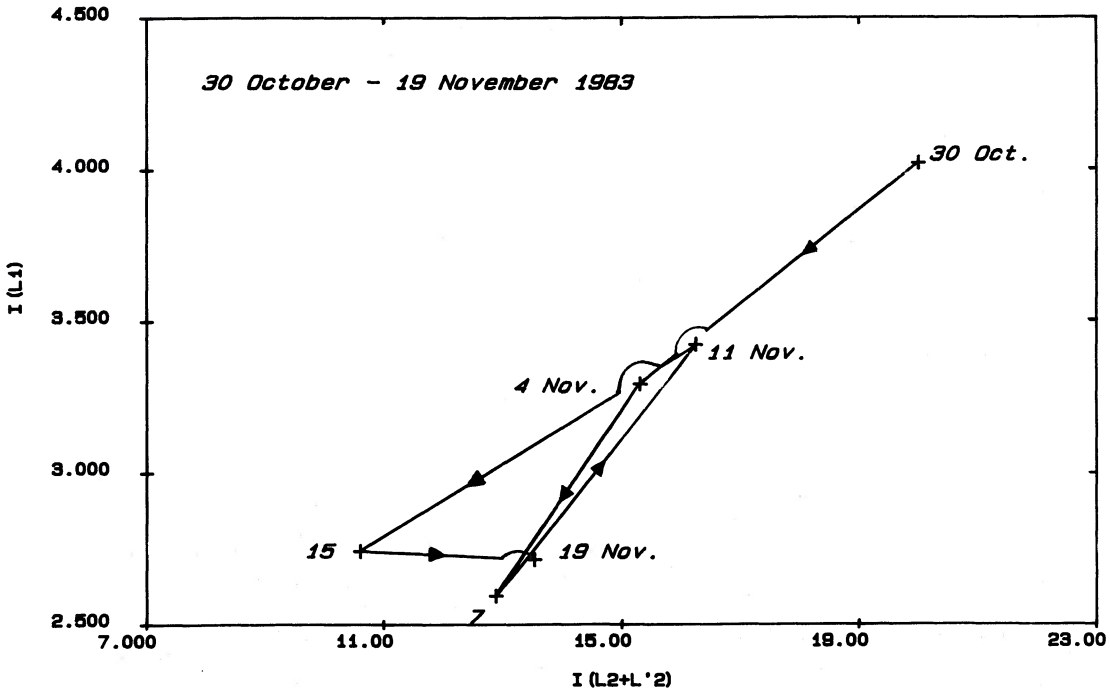

FIG. 10*b*

FIG. 10.—As in Fig. 9, we plot here intensities of L1 λ1518 line and L'2 λ1576 + L2 λ1594 blend but only for well-sampled 1981 April–July and 1983 October–November episodes. Error bars are now omitted for clarity, and sense of time is indicated by arrows connecting contiguous epochs. Both diagrams show that, on short and medium time scales (days to months), intensities of L1 and L2 + L'2 are well correlated and that any lag is very short. This constrains the jet to be almost in plane of sky and sets an upper limit of 8 lt-day to distance of L1 and L2 + L'2 emitting obstacles to origin of jet. Note that vertical scale differs in (*a*) and (*b*).

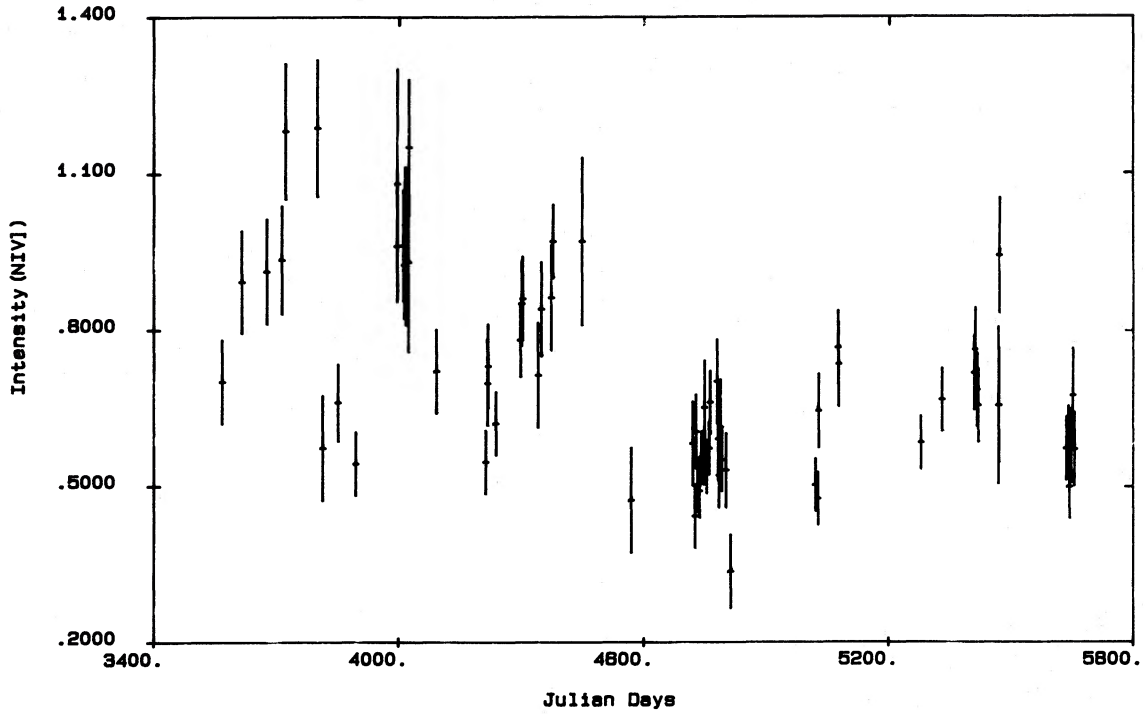

FIG. 11*a*

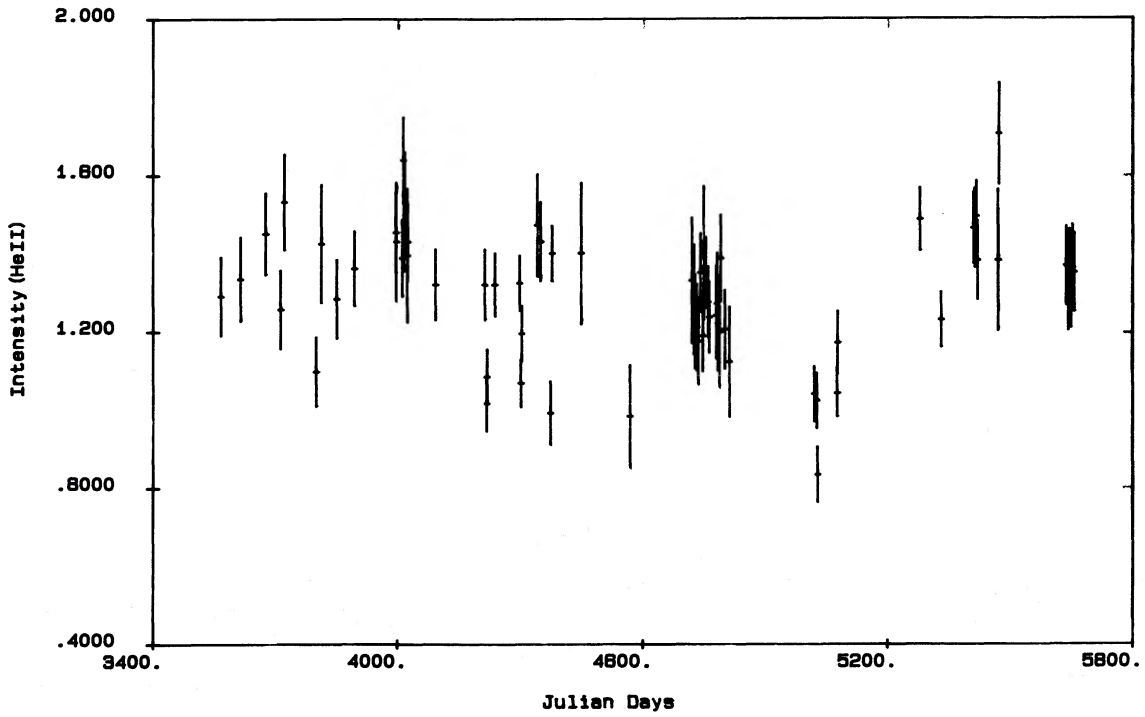

FIG. 11*b*

FIG. 11.—Light curves of N IV] λ1485 (*a*), the He II λ1640 core (*b*), and O III] λ1663 (*c*). The N IV] line shows variations which are occasionally strong and rapid, while He II core and O III] lines experience only mild variations and on time scales longer than ~250 days, suggesting that they originate from an extended region, the ILR (see text).

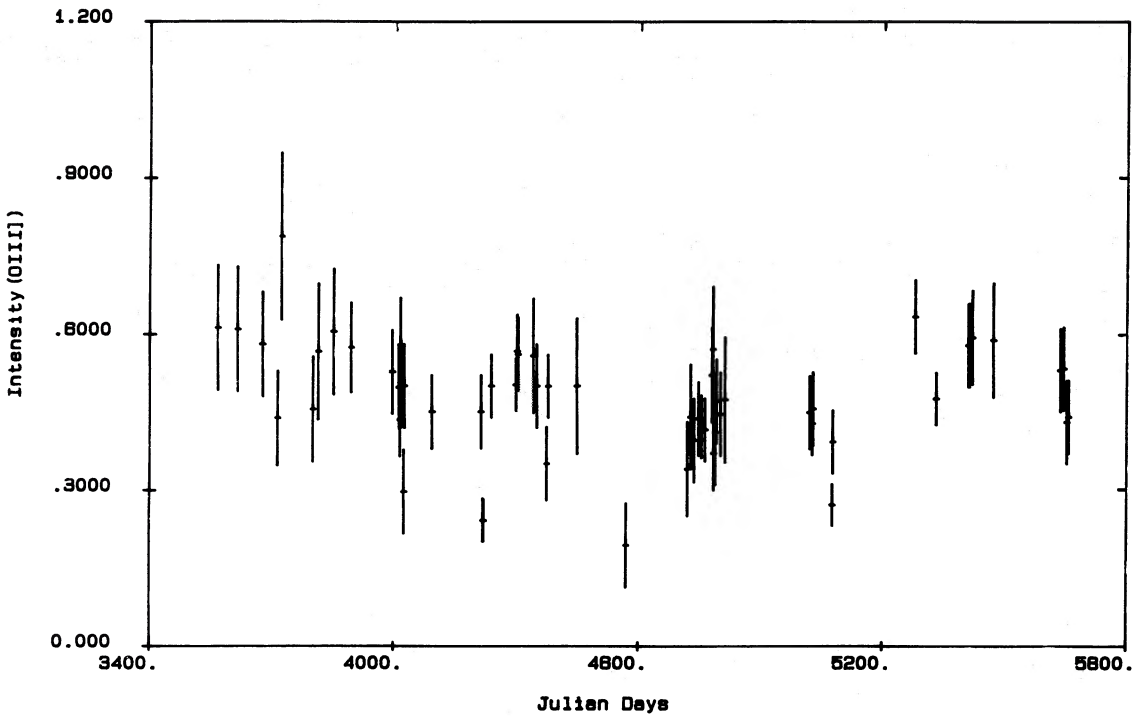

FIG. 11*c*

5.7 σ level. For O III], one finds $D(I) = 2.3$, but at the 3.3 σ level only, while the range of the He II core is definitely smaller: $D(I) = 0.86 \pm 0.23$ (5.3 σ). There are no significant variations of the He II core and O III] line over time scales shorter than $\sim$250 days. On the other hand, the N IV] line intensity dropped by a factor of $\sim$2 (at the 3.7 σ level) in the interval 1978 October 19–31. This decay occurred similtaneously with a factor of $\sim$3 decrease of the continuum flux.

As can be seen in Figure 12, the intensity of the N IV] λ1485 is correlated with the continuum (at the 99.9% level). A linear fit to the data ($r = 0.71$, reduced $\chi^2 = 2.1$) yields

$$I_0(\text{N IV}]) = (0.20 \pm 0.01)F(1450) + (0.49 \pm 0.01) .$$

This relation predicts a nonzero N IV] intensity when the continuum vanishes. We interpret this residual flux as being emitted by material which lies too far away from the continuum source to respond to the rapid variations in the rate of ionization. Since the mean N IV] intensity, averaged over the entire 1978–1983 episode is $(0.7 \pm 0.2) \times 10^{-13}$ ergs cm^{-2} s^{-1} Å^{-1}, this constant or slowly variable component accounts for 70% of the total N IV] flux. Given the N IV] line width, it presumably arises in the ILR, as was pointed out in § III*d*.

Neither the O III] λ1663 nor the He II λ1640 core intensities are correlated with the continuum flux ($r = 0.13$ and 0.05, respectively). On the other hand, the O III] and He II core intensities are correlated one with the other at the 99.9% level (see Fig. 13). Moreover, the regression line ($r = 0.60$, $\chi^2 = 1.2$) goes through the origin:

$$I_0(\text{O III}]) = (0.36 \pm 0.01)I_0(\text{He II}) + (0.00 \pm 0.02) .$$

The simplest explanation is that the bulk of the energy radiated by the two lines comes from the same region. As a matter of fact, taking into account the 1661.2–1666.5 Å doublet separation, the intrinsic O III] line width is $\sim$1540 km s^{-1}, i.e., very close to that of the He II core.

As explained in § II*a*, the bulk of the C III] λ1908 line flux is also contained in 1600 km s^{-1} FWHM and barely variable core. We therefore conclude that the He II core, C III] core, O III], and $\sim$70% of the N IV] line intensities come from the same physical region, the ILR. The same gas should also be responsible for the residual 1560 km s^{-1} C IV core emission line predicted by the FWHM (C IV–C) versus $F(1450)$ correlation found in § III*d*. Because there are no significant variations of the He II core on time scales shorter than $\sim$250 days, we tentatively assigned a radius of 250 lt-day to the ILR.

IV. INTERPRETATION AND DISCUSSION

a) Velocity versus Radius

Table 8 summarizes the "radii" R of the various emitting regions identified in § III, together with the width of the corresponding line(s), while in Figure 14 we plot these FWHMs as a function of $R^{-1/2}$. The two quantities are *linearly* correlated at the 99.7% confidence level ($r = 0.997$). If one adds the point corresponding to the narrow-line region (NLR) of NGC 4151, the significance of the correlation increases to 99.9%. The radius of the NLR was taken to be 1.″6—i.e., that of the brightest and most central [O III] λ5007 cloud I of Ulrich (1973)—

TABLE 8

RADIUS VERSUS VELOCITY FOR THE VARIOUS LINE EMITTING REGIONS

Emitting Region	Radius (lt-day)	FWHM (km s^{-1})
C IV λ1550 broad	5^{+4}_{-2}	14600
He II λ1640 broad	15 ± 2	8600
C IV λ1550 Core	25 ± 5	>5600
ILR[a]	250 ± 50	1600
NLR	1.8×10^5	240

[a] Intermediate line region (see text).

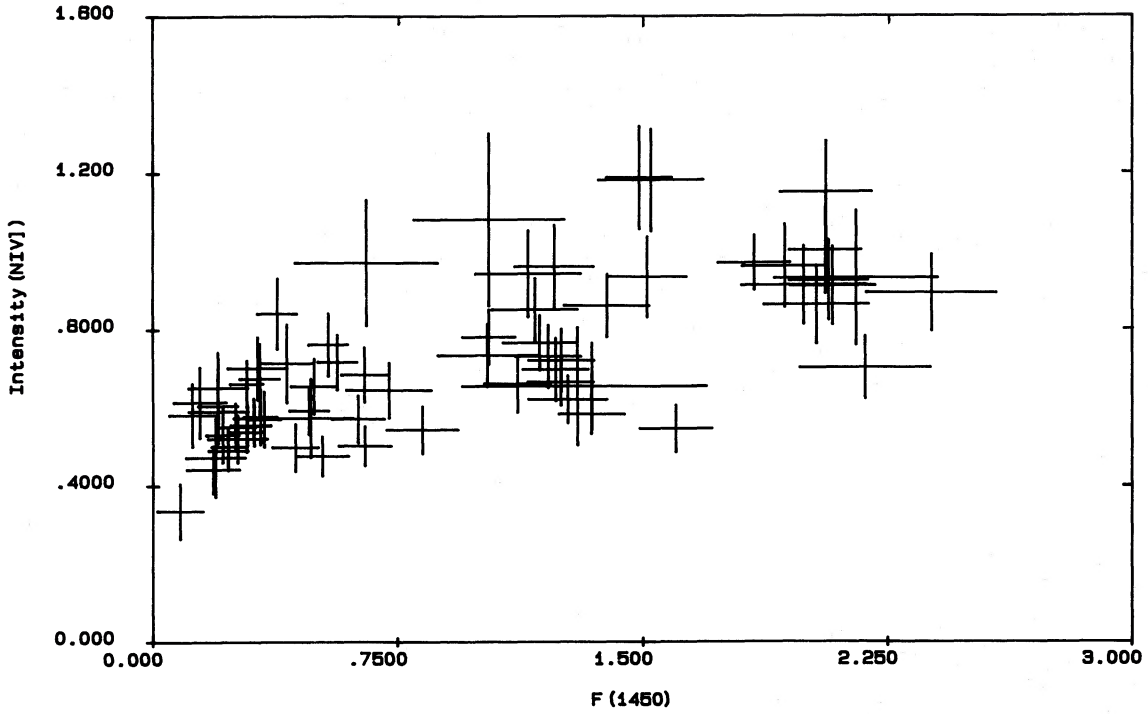

FIG. 12.—Peak intensity of N IV] λ1485 line vs. intensity of continuum at 1450 Å. The two quantities are weakly correlated, but best-fit regression line does not go through origin. Interpretation is that N IV] λ1485 line contains both a variable component which presumably originates close from continuum source and a more stable contribution which, given line width, originates in extended ILR. On average, ILR component accounts for about two-thirds of N IV] line flux.

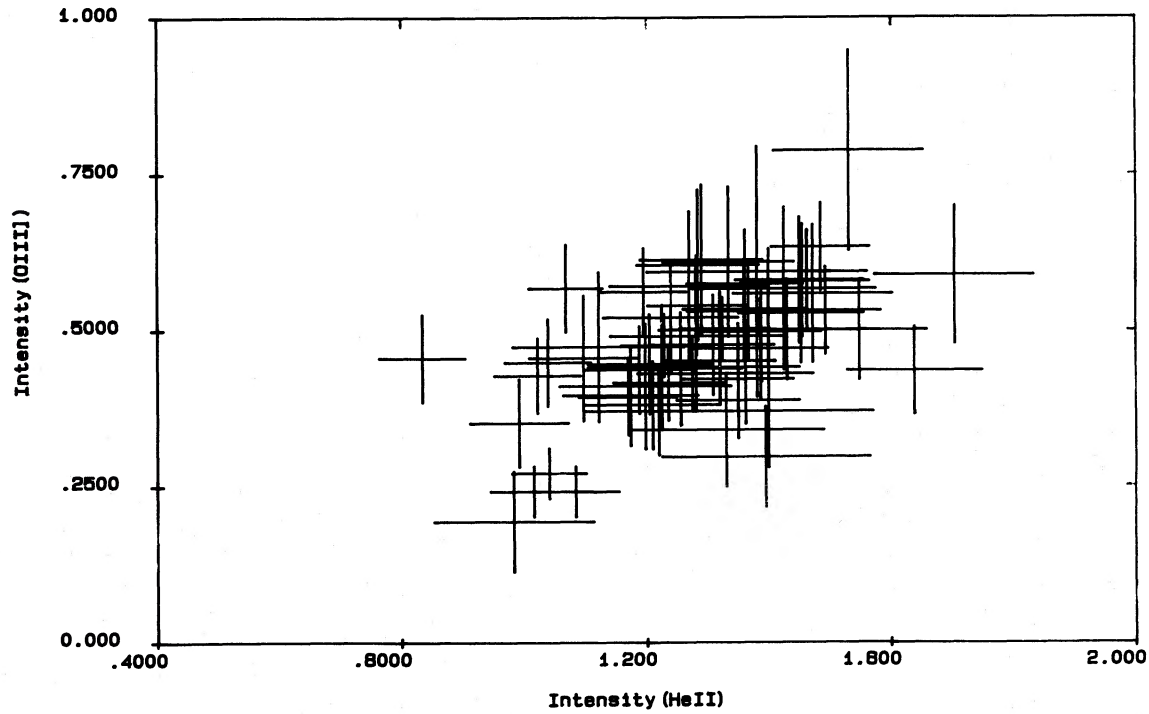

FIG. 13.—Peak intensity of O III] λ1663 vs. that of He II λ1640 emission core. Even though their variations are small, the two quantities are clearly correlated. We interpret this as further evidence that both lines come from ILR.

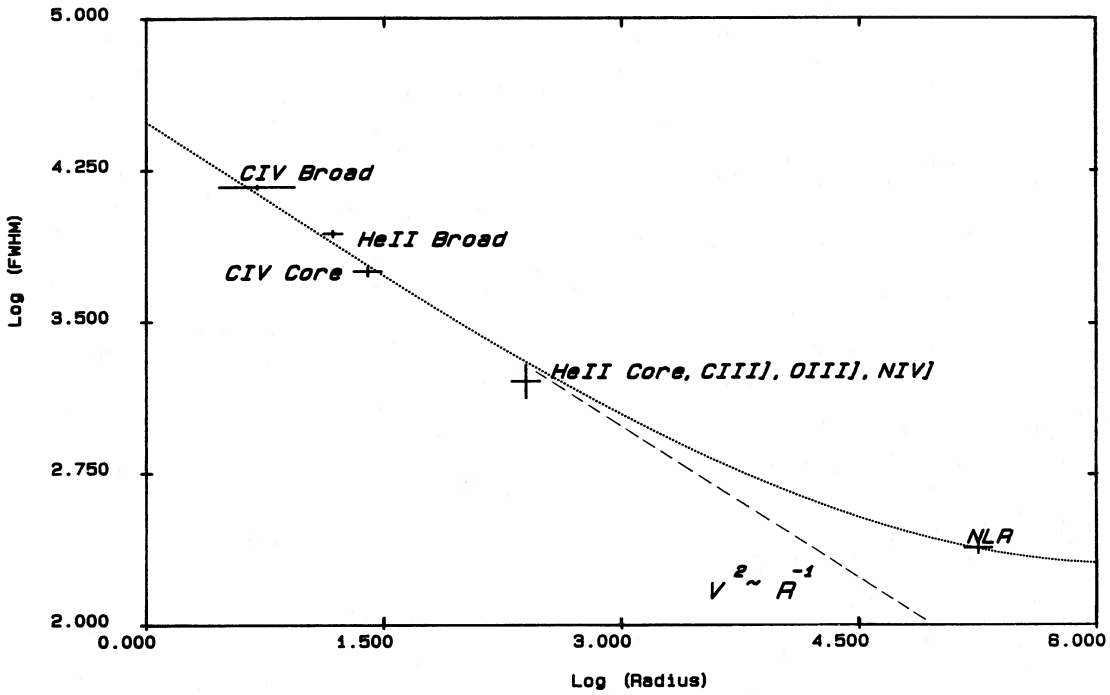

FIG. 14.—FWHM of various lines (in units of 100 km s^{-1}) as function of inverse square root of "radius" of corresponding emitting regions (in lt-day) plotted with associated error bars (see text) on logarithmic scale. This shows excellent linear correlation, which suggests that velocity of BLR gas is Keplerian. Slope of best-fit regression line (*dashed*) yields $\sim 4 \times 10^7\ M_\odot$ for central mass inside BLR. Linear regression including NLR also yields a very good fit (*dotted line*). However, it predicts a nonzero velocity at infinity. This shows that narrow-line gas feels a larger central mass than do broad-line clouds.

which corresponds to $\sim$500 lt-yr. Its velocity dispersion, expressed as a FWHM, is 240 km s^{-1} (Pelat and Alloin 1982). Assuming errors of 300 km s^{-1} on the other line widths and a relative error of 20% on all distances, a linear fit to the data yields (FWHM in km s^{-1} and R in lt-day

$$\text{FWHM} = (33800 \pm 3100)R^{-1/2} - (600 \pm 490)\,,$$

without the NLR ($\chi^2 = 0.44$), and

$$\text{FWHM} = (30300 \pm 1700)R^{-1/2} + (166 \pm 20)\,,$$

when the NLR point is included in the regression ($\chi^2 = 1.20$). This shows that, to a very good approximation, the run of velocity with distance is Keplerian at least up to a radius of $\sim$1 lt-yr. However, the fact that the second of these relationshi-s predicts a velocity at infinity which is significantly different from zero implies that the gravitational potential as seen by the NLR gas is larger than that which the BLR clouds feel, as was already found by Ferland and Mushotzky (1982).

The best study of the spectroscopic variability of NGC 4151 in the optical range is that of Antonucci and Cohen (1983). The time scales they find for He II λ4686, Hγ and possibly Hβ are of the order of 7 to 10 days and definitely longer for Hα. These figures are similar to those inferred for the UV lines. It is unfortunate that Antonucci and Cohen do not quote the line widths as doing so would have allowed us to further check the vlidity of the $V \sim R^{-1/2}$ law which we infer from the UV data.

The linear coefficients of the best-fit regression lines (equal within the uncertainty) yield a direct estimate of the central mass M. Since we have used Gaussians to fit the profiles, we have implicitly assumed that macroturbulence is the main source of line broadening, in qualitative agreement with the conclusion of Paper III. The most probable turbulent velocity is given by $V_{\text{turb}} = 0.6$ FWHM, which yields $M = (3.7 \pm 0.5) \times 10^7\ M_\odot$. This calculation relies on the same physical model as that in Paper III, i.e., the BLR clouds are treated as test particles along randomly oriented parabolic orbits. This value of M is an order of magnitude smaller than that found in Paper III because (1) the more accurate distance estimates used here are systematically smaller and (2) we have used V_{turb} instead of the half width at zero intensity which is difficult to measure and, inappropriately, is a maximum rather than a mean.

The fastest variations recorded so far indicate a (two-folding) dimension of $\sim$10 lt-hours for the X-ray source in NGC 4151 (Paper VI), which corresponds to 90 Schwarzschild radii for a $4 \times 10^7\ M_\odot$ mass. This is quite a reasonable value as far as AGN models with accretion onto a central black hole are concerned (see, e.g., Maraschi, Rosario, and Treves 1982).

The tight relationship between radius and velocity is a potentially important tool for the diagnosis of the BLR gas. *Isovelocity* (i.e., monochromatic) emission-line intensity ratios can then be used to constrain photoionization models and derive the run of physical conditions as a function of distance to the continuum source.

b) *Physical Conditions*

In the optical spectrum of NGC 4151, Pelat and Alloin (1982) detected a "broad" 1750 km s^{-1} FWHM [O III] λ5007 component underlying the narrow NLR emission core and accounting for 45% of the total flux in the line. Given its width, this feature presumably arises in the ILR. The critical density above which the upper level of the 5007 Å transition starts being collisionally de-excited is 6.5×10^5 cm^{-3}. This implies that the density inside the ILR cannot be much larger than a

few multiples of 10^7 cm^{-3}. The average intensity ratio of O III] λ1663 over broad [O III] λ5007 is 0.12 with a 30% uncertainty. If the reddening of the ILR is the same as that of the NLR—i.e., $E(B-V) = 0.24$, as inferred from the [S II] line ratio (Wampler 1971)—the 1663/5007 ratio becomes 0.31 after correction for reddening (Seaton 1979). Boksenberg *et al.* (1975) found log $(T_e) = 4.07 \pm 0.03$ K for the temperature of the gas in the NLR of NGC 4151. If this applies also to the ILR, one can use Table 5 of Nussbaumer and Storey (1981) to infer log $(N_e) = 7.2 \pm 0.2$ cm^{-3} for the density. Using instead $E(B-V) = 0.05$, corresponding to galactic reddening only yields log $(N_e) = 6.8$, whereas varying the temperature between 10^4 and 1.3×10^4 K changes the density to log $(N_e) = 7.5$ and 6.7, respectively. We conclude, therefore, that *within a factor of 2 of uncertainty, the density inside the ILR is* 10^7 cm^{-3}. This is three orders of magnitude higher than the density of the NLR [log $(N_e) = 4.1$; Boksenberg *et al.* 1975] but still far below the canonical $10^{9.5}$ value generally accepted for the BLR of AGNs. By its dimension, velocity, and density, the ILR represents some kind of transition between the narrow-line and the broad-line gas. Penston *et al.* (1984) derived a lower limit of 2.2×10^5 cm^{-3} for the density of the [Fe X] λ6374 line emitting region in NGC 4151, which suggests that the Fe^{+9} feature arises in the ILR. The λ6374 line is also possibly variable, though this needs confirmation. We note that the width (380 km s^{-1}) and time scale for variability ($\sim$3 yr) of this line do not fit into the velocity versus radius correlation found earlier. However, the λ6374 feature is weak and blended with the much stronger [O I] λ6300 line, which makes the above measurements rather uncertain.

On the other hand, several arguments suggest that the density of the high-velocity material in NGC 4151 exceed log $(N_e) = 9.5$:

1. As pointed out in Paper III, the fact that the intensity of the broad C IV line increases with the continuum sets an upper limit to the ionization parameter, U, of the inner gas. (At higher U values the C IV intensity would decrease with increase of U, as the C^{+3} ions are transformed into C^{+4}.) This in turn constrains N_e to be of the order of 10^{11} cm^{-3} or larger. Moreover, Figure 2 of Ferland and Mushotzky (1982) shows that the intensity of the C IV line increases together with the intensity of the continuum only as long as the ionization parameter remains lower than log $(U) \sim -1$. However, already at log $(U) \sim -2$, the C IV emissivity enters a plateau where it starts increasing much more slowly than linearly. The fact that the regression line of Figure 4 goes through the origin shows that we are generally on the linear section of the C IV intensity versus U curve, hence below log $(U) = -2$. However, the former correlation between I_0(C IV–B) and the continuum intensity becomes statistically insignificant (level of confidence drops to 93%) if the analysis is restricted to those epochs when $F(1450)$ exceeds 1×10^{-13} ergs cm^{-2} s^{-1} Å^{-1}. This suggests that during the high states of NGC 4151, the C IV–B emissivity enters the plateau regime, i.e., log $(U) \sim -2$. This immediately translates into $N_e \approx 5 \times 10^{11}$ cm^{-3} for the broad C IV emitting gas, with a large uncertainty mainly due to the unknown shape of the NGC 4151 continuum beyond the Lyman edge.

2. For velocities larger than $\sim$1600 km s^{-1}, the C IV λ1550/Lyα λ1216 monochromatic intensity ratio is larger than 10, whereas photoionization models predict a ratio of 0.65 (e.g., Kwan and Krolik 1981; Ferland and Mushotzky 1982). Both large densities and high temperatures are required to enhance C IV over Lyα (Kwan and Krolik 1981).

3. The weakness or absence of significant emission from C III] λ1908 in the velocity range above 3000 km s^{-1} (FWHM) where *both* C IV λ1550 and Mg II λ2800 are still strong indicate densities in excess of 10^{10} cm^{-3} (Paper III). The same argument, based on critical densities for collisional de-excitation, can also be applied to the O III] λ1666.2 and N IV] λ1468.5 lines to infer lower limits for log (N_e) of 10.7 and 10.9, respectively.

4. The absence of He II λ1640 emission in the velocity (FWHM) range 8600–14,600 km s^{-1} where C IV λ1550 is strong is more difficult to understand, but probably also implies the existence of both high densities *and* high temperatures. This is essentially the same problem as that raised by the disappearance of the He II–B feature at low or intermediate states when C IV–B is still present (see § IIIc). In the framework of photoionization models with a density of $10^{9.5}$ cm^{-3} and temperature of $\sim 10^4$ K, the C IV λ1550 line is collisionally excited, whereas He II λ1640 is formed by recombination. Since He^{+2} and C^{+3} require almost the same ionization energy, $\sim$50 eV, it is difficult to conceive of a mechanism which could drastically enhance the C IV λ1550/He II λ1640 intensity ratio over its theoretical value. Intuitively, the most promising way to do this is to raise both the density and the temperature of the gas so as to boost collisional excitation over recombination. It is difficult to be more quantitative in the absence of detailed photoionization calculations, and theoreticians are urged to include a high-density/high-ionization parameter region in their models of the BLR of Seyfert galaxies.

If N_e actually reaches 10^{11} cm^{-3}, the internal density of a cloud increases by a factor of 10,000 from the ILR to the C IV–B emitting region. This yields a run of density with radius which is faster than the $R^{-3/2}$ law which would naively be expected from mass conservation in a free-fall spherically symmetrical and homogeneous accretion flow with an $R^{-1/2}$ velocity law as found earlier. This is an additional constraint which models of active galaxies and quasars will have to take into account. Suppose, for instance, that the BLR clouds are pressure confined by a hot ambient medium, as postulated by Krolik, McKee, and Tarter (1981); the above run of density would then imply that the temperature of the hot phase increases faster than the virial temperature (which goes as R^{-1}). Under such circumstances, the gas is probably forced to expand (e.g., Mathews and Capriotti 1985).

c) *About the Velocity Field*

We now turn to the correlation found in § III*b* between the wavelength and the intensity of the broad C IV component. In a very general sense, an asymmetry implies radial motions together with some kind of obscuration, either infall with dust at the back of each cloud, or outflow with a central region hiding clouds on the far side. The infall model, however, faces serious difficulties:

1. The dust which it requires cannot survive at a few light-days from the continuum source (Ferland and Mushotzky 1982.

2. Moreover, if dust absorbs, it must also reradiate, and one would therefore expect to see large amplitude and rapid variations of the near IR flux. These have never been observed so far (Lebofsky and Rieke 1980; Penston *et al.* 1974).

3. If anything, the dust-to-gas ratio is anomalously low in Seyfert galaxies in general and in NGC 4151 in particular, as

can be inferred from a comparison of the X-ray absorbing column with the equivalent width of the 2200 Å dust signature.

On the contrary, the outflow model seems more natural since there is already direct evidence of outward motions in the form of blueshifted absorption lines in the spectrum of NGC 4151. In the outflow scheme, the central obscuration could, for instance, be due to an optically thick accretion disk (AD). Observational evidence in favor of the existence of ADs in AGNs, or at least of a flattened configuration for the gas, has recently been increasing (Antonucci 1984; Rudy *et al.* 1983; Malkan and Sargent 1982; Cohen 1983). On the theoretical side, a thick AD or torus may be useful to collimate the radio jet in NGC 4151 (see Rees *et al.* 1982). In addition, an AD provides a tank of material to continuously replenish the outflow. Indeed, a certain class of models predicts that AGN disks, if they exist, will, under certain conditions, emit a wind which is made of material boiled off from the chromosphere of the disk by hard X-rays (see Begelman, McKee, and Shields 1983).

Assuming that a disk is the actual source of obscuration, the intensity-dependent asymmetry of the C IV profile is readily explained. When the continuum is faint, only the innermost expanding shell is illuminated. Its far side being partially hidden, the C IV–B line has a net blueshift. As the continuum intensity increases, the ionization front propagates outward, and regions farther out start emitting C IV photons as well. Let us now assume that the external radius of the disk is not much larger than 5 lt-day, in such a way that the AD encompasses *only* the innermost gas shell, i.e., the one which is responsible for the broad residual C IV line seen at low states. Then, as the burst develops and the ionization front propagates outward, the fraction of the C IV–B line flux which comes from the far receding side of the nebula increases. As a result, when the line gets stronger it becomes less asymmetrical. Note however, that the far side of the innermost shell remains permanently hidden. Since this contains the highest recession velocity material, the C IV–B line is never redshifted.

To gain some further insight into the geometry of the system, let us make the reasonable assumption that the disk is perpendicular to the L1/L2 exciting jet. The AD is therefore seen almost edge-on, at an inclination $i = 15°$ from the LOS.

In principle, because the far side of the C IV–B emitting shell is partially hidden and most of the emission comes from material which is located in front of the source of continuum, the 5 day time delay measured in § III*b* underestimates the true value of the radius. In practice, however, the correction factor, $1/\cos i$, is sufficiently close to 1 to be neglected.

Assuming spherical symmetry, and if the line emissivity is proportional to the surface area of the emitting shell, the obscuration by the disk is expected to enhance the blue wing by a fraction $f = 2i/(90 - i) = 0.40$ of the flux in the red wing. Interestingly, the excess energy which is required to account for the observed blue asymmetry of the residual C IV–B line corresponds to $f = 39\%$.

The blue excess is expected to be spread over all frequencies corresponding to velocities in the range 0 to $-V$, with a maximum at $-V$, where V is the expansion velocity of the shell. The shift of the residual C IV–B line, -20, Å, therefore provides a direct estimate of the outflow velocity, $V \approx 4000$ km s^{-1}.

Since our model constrains the external radius of the disk R_d to be of the order of 5 lt-day, the obstacles where the L2 line is excited by the jet remain visible to the observer. In fact, given the inclination of the disk and the upper limit derived earlier for the distance of the obstacles to the origin of the jet (§ III*f*), the condition that L2 be visible only constrains R_d to be smaller than 15 lt-day. Thermal radiation from the disk could account for part or the whole of the UV continuum. For instance, a 10^4 K disk with a 5 lt-day radius will deliver at Earth a 1450 Å flux of 6×10^{-14} ergs cm^{-2} s^{-1} Å^{-1}. This figure takes into account the inclination of the AD, external reddening ($E[B-V] = 0.05$) and assumes that the disk radiates like a blackbody.

The present data are therefore consistent with the hypothesis that the residual broad C IV line originates in a shell whose radius is ~ 5 lt-day and which expands at a velocity $V \sim 4000$ km s^{-1}. Since the velocity of the absorption line gas—located much farther out, on the outskirt of the ILR (Paper IV)—is 800 km s^{-1}, the obvious conclusion is that *the outflow is decelerated.* Radiation-driven winds cannot be decelerated, unless the gas becomes shielded beyond a certain distance from the source of continuum. Moreover, it is easy to show that radiation pressure fails by almost two orders of magnitude to provide enough momentum to counteract the gravitational binding in NGC 4151. In fact, the observed decrease in radial velocity with radius suggests some kind of ballistic type of flow. The mechanism responsible for the initial push is unknown, but could be related to the jet phenomenon.

It is worth reemphasizing here that $V \ll$ FWHM (C IV–B). In other words, radial motions are *not* the main source of line broadening. In fact, the intensity-dependent asymmetry of the C IV line represents only a minor perturbation to a profile which basically remains symmetric. This property, together with the gross similarity of the line shapes during the low and high states of NGC 4151, led us to conclude in Paper III that the velocity field is dominated by chaotic motions. A plausible scenario mentioned earlier is that of clouds with parabolic orbits having random orientations with respect to the line of sight. It is unclear to what extent the outflow and the chaotic motions are related, or if they affect different parts of the flow. It could be, for instance, that the assembly of clouds undergoes expansion globally, the radial movement being superposed on the orbital motion of individual clouds. Alternatively, the main BLR with its comet-like clouds could be confined to a flattened configuration, while the expanding gas above and below that plane either represents material which escaped collimation into the jet, or gas which evaporates from the chromosphere of the disk.

It also remains to be explained why the expanding gas is seen in absorption only at large radii. The only plausible explanation for this is that the covering factor of the continuum source by the clouds somehow increases with distance. We can briefly mention one scenario which, building on the results of Papers IV and VI, places the absorption region at the interface between the ILR and the NLR. Inside the BLR, as is usually the case for AGNs, the emission-line clouds intercept only a small fraction of the sky as seen from the continuum source. However, radially moving clouds tend to pile up on the NLR obstacle and eventually form a screen. The strong shock-induced heating which this scenario predicts would account for the nonvariable soft X-ray excess detected with *EXOSAT* (Paper VI) and the [Fe X] λ6374 emission (Penston *et al.* 1984). seen in the optical range. As a final remark, it is unlikely that the region where the wind is accelerated can be detected spectroscopically, since this inner gas is probably too hot to produce UV or optical emission lines. It will be interesting,

however, to monitor the profile of the O VI λ1035 emission line or that of the iron feature around 6.4 keV (e.g., Matsuoka *et al.* 1986) when the next generation of space facilities such as *LYMAN* or *AXAF* become available.

V. SUMMARY

The careful study of the C IV λ1550 line profile and its variation over 6 yr and 69 different epochs of observation has led to several new results which are now summarized:

1. The underlying continuum over the 1430–1720 Å range is extremely flat with a frequency spectral index of -0.17 ± 0.12, interestingly close to that of the polarized continuum in the optical. There is no evidence for variation of this index with time.

2. A large fraction of the C IV line flux is contained in a very broad component (FWHM = 14,600 km s^{-1}) whose response time to the continuum intensity variations indicates that it originates in a region $\sim$5 lt-day in radius. The density of the gas reaches at least 10^{11} cm^{-3} in this innermost region, as can be inferred from (*a*) the absence of O III] λ1663, N IV λ1485, and C III] λ1908 emission in that range of velocity, and (*b*) the very fact that the emissivity of the line keeps increasing with increasing U. The absence of Lyα λ1216 and He II λ1640 emission at large velocities also suggests the existence of high density *and* temperatures.

3. Similarly, a broad (8600 km s^{-1} FWHM) component carries much of the He II λ1640 line flux and is emitted by a region whose radius is 15 ± 2 lt-day.

4. Contributions to the core of the C IV λ1550 line come from both a variable and a constant component. The variable part originates in a region whose radius is $\sim$25 lt-day and whose velocity dispersion is at least 5500 km s^{-1}.

5. The constant contribution to the C IV λ1550 line core originates in the same region which emits the He II λ1640 core, the O III] λ1663 line, most of the N IV] λ1485 and C III] λ1908 flux, as well as the "broad" [O III] λ5007 component seen in the optical. In this subregion, $\sim$250 lt-day in radius, the density of the gas is $\sim 10^7$ cm^{-3} and its velocity dispersion (FWHM) 1600 km s^{-1}. It probably represents the long sought transition between the BLR and NLR gas and was therefore named ILR for intermediate width line region.

6. The velocity dispersion in these different regions is linearly correlated with the inverse square root of their radii, which is consistent with Keplerian motion of the BLR gas. Our best estimate of the central mass is $(3.7 \pm 0.5) \times 10^7\ M_\odot$. The NLR appears to see a larger central mass than the broad-line gas.

7. The velocity field within the BLR is dominated by chaotic motions. However, we also find evidence for radially moving gas in the form of an intensity dependent asymmetry of the C IV line profile. The absence of rapid variations in the near IR, together with theoretical reasons favor the expansion hypothesis. If, as seems plausible, the same gas is also responsible for the many broad, blueshifted, and variable absorption lines seen in the ultraviolet and the optical range, then the outflow is decelerated, its velocity dropping from 4000 km s^{-1} at 5 lt-day to 800 km s^{-1} at $\sim$1 lt-yr from the center. This scenario also requires the existence of some central obscuration mechanism so as to hide part of the receding gas. We note that a thick accretion disk, a few light-days across, could provide both the obscuration and a reservoir of material to replenish the wind.

8. In contrast with the other emission lines, the intensity of the *L*1 λ1518 and L2 λ1594 unidentified features does *not* correlate with that of the continuum. Still, their rapid variations led us (Paper V) to propose that they are satellite C IV lines excited by the two-sided radio jet. The facts that L1 and L2 vary in phase and that any lag, if present, is smaller than 4 days constrain the jet to lie very close to the plane of the sky and the obstacle to be within 8 lt-day from the origin of the jet. The small velocity difference between L1 and L2 yields an inclination of 75° with respect to the line of sight, thereby confirming that the jet is close to the plane of the sky. If, as theoretical considerations suggest, the jet is funneled by and therefore perpendicular to a thick accretion disk, or torus, then a loose upper limit of 15 lt-day is obtained for the disk radius from the fact that the L2 emitting obstacle remains visible. This limit is compatible with the size of the central obscuring screen.

We thank an anonymous referee for his useful and constructive comments which improved the present article.

APPENDIX

ABOUT THE APPLICABILITY OF CROSS-CORRELATION TECHNIQUES TO LIGHT CURVES

We have applied cross-correlation (CC) techniques to the C IV–B and continuum light curves in an attempt to measure the characteristic lag of I_0(C IV–B) with respect to F(1450) (see § III*b*). Our conclusion is that such techniques are not applicable here and do not improve upon the results obtained by visual comparison of the light curves.

To be reliable, CC techniques require that the curves to compare (1) are well sampled and, in particular, that they do not have large gaps and (2) contain several sharp and time-resolved "events" (peaks or dips). Neither conditions are fulfilled by the present data.

Under such circumstances, one has first to interpolate between the data points of the light curves prior to cross-correlating them. Even for our best covered episodes—when the sampling interval is typically 4 days—this already introduces uncertainties given that (1) the continuum is known to vary occasionally on a time scale of $\sim$2 days (Paper II), and (2) the choice of a method of interpolation is arbitrary. But the uncertainty becomes unacceptably large when the interpolation is performed over periods of several months. Indeed, this amounts to inventing large pieces of data whose weight in the final results will be larger than that of smaller but well-covered episodes. On the other hand, the few well-sampled intervals at our disposal lack fully resolved events, and by themselves are not suitable for CC techniques.

As an illustration, we show in Figure 5*d* the CC function of the entire 1978–1983 C IV–B and continuum light curves. The autocorrelation curve of I_0(C IV–B) is also given for reference. Linear interpolation has been used to fill in gaps, and the light curves were both normalized in such a way that their mean and rms deviations are 0 and 1, respectively. The maximum of the CC function

is at $D = -9$ days. Though D has the correct sign and order of magnitude, the peak is so broad that it is difficult to assess the error attached to such a delay.

Experiments have been run to test the stability of this solution by changing, for instance, the method of interpolation, or selecting subsamples of the light curves. It was found that D can easily vary by several days (up to four). Therefore, only a limited significance should be attached to the earlier estimate of 9 days.

REFERENCES

Antonucci, R. R. J. 1984, *Ap. J.*, **278**, 499.
Antonucci, R. R. J., and Cohen, E. D. 1983, *Ap. J.*, **271**, 564.
Baldwin, J. A. 1976, *Ap. J.*, **214**, 679.
Begelman, M. C., McKee, C. F., and Shields, G. A. 1983, *Ap. J.*, **271**, 70.
Blandford, R. D., and McKee, C. F. 1982, *Ap. J.*, **255**, 413.
Bromage, G. E., *et al.* 1985, *M.N.R.A.S.*, **215**, 1 (Paper IV).
Boksenberg, A., *et al.* 1975, *M.N.R.A.S.*, **173**, 381.
Booler, R. V., Pedlar, A., and Davies, R. 1982, *M.N.R.A.S.*, **199**, 229.
Cohen, R. 1983, *Ap. J.*, **273**, 489.
Ferland, G. J., and Mushotzky, R. F. 1982, *Ap. J.*, **262**, 564.
Johnston, K. J., *et al.* 1982, *Ap. J.*, **262**, 61.
Khachikian, E. Y., and Weedman, D. W. 1974, *Ap. J.*, **192**, 581.
Krolik, J. H., McKee, C. F., and Tarter, C. B. 1981, *Ap. J.*, **249**, 422.
Kwan, J., and Krolik, J. H. 1981, *Ap. J.*, **250**, 478.
Lebofsky, M. J., and Rieke, G. H. 1980, *Nature*, **284**, 410.
Malkan, M. A., and Sargent, W. L. 1982, *Ap. J.*, **254**, 22.
Maraschi, L., Rosario, R., and Treves, A. 1982, *Ap. J.*, **253**, 312.
Mathews, W. G., and Capriotti, E. R. 1985, in *Astrophysics of Active Galaxies and Quasistellar Objects*, ed. J. S. Miller (Santa Cruz: Lick Observatory, University of California, Santa Cruz), p. 185.
Matsuoka, M., *et al.* 1986, *Pub. Astr. Soc. Japan*, **38**, 285.
Nussbaumer, H., and Storey, P. 1981, *Astr. Ap.*, **99**, 177.
Pelat, D., and Alloin, D. 1980, *Astr. Ap.*, **81**, 172.
———. 1982, *Astr. Ap.*, **105**, 335.
Penston, M. V., *et al.* 1974, *M.N.R.A.S.*, **169**, 357.
———. 1979, *M.N.R.A.S.*, **189**, 45P.
———. 1981, *M.N.R.A.S.*, **196**, 857 (Paper I).
———. 1984, *M.N.R.A.S.*, **208**, 347.
Perola, G. C., *et al.* 1982, *M.N.R.A.S.*, **200**, 293 (Paper II).
———. 1986, *Ap. J.*, **306**, 508. (Paper VI).
Rees, M. J., *et al.* 1982, *Nature*, **295**, 17.
Rudy, R. J., *et al.* 1983, *Ap. J.*, **271**, 59.
Schmidt, G. D., and Miller, J. S. 1980, *Ap. J.*, **240**, 759.
Seaton, M. J. 1979, *M.N.R.A.S.*, **187**, 73P.
Snijders, M. A. J., *et al.* 1987, in preparation.
Ulrich, M. H. 1973, *Ap. J.*, **181**, 51.
Ulrich, M. H., *et al.* 1984, *M.N.R.A.S.*, **206**, 221 (Paper III).
———. 1985, *Nature*, **313**, 745 (Paper V).
Veron, P., Veron-Cetty, M. P., and Tarenghi, M. 1985, *Astr. Ap.*, **150**, 317.
Wampler, E. J. 1971, *Ap. J.*, **164**, 1.
Wills, B. J., Netzer, H., and Wills, D. 1985, *Ap. J.*, **288**, 94.
York, D. 1966, *Canadian J. Phys.*, **44**, 1079.

A. ALTAMORE and G. C. PEROLA: Istituto Astronomico, Universita di Roma, Via Lancisi 29, 00162 Roma, Italy

A. BOKSENBERG, M. V. PENSTON, and M. A. J. SNIJDERS: Royal Greenwich Observatory, Herstmonceux Castle, Hailsham, East Sussex BN27 1RP, UK

G. E. BROMAGE: Astrophysics Group, Rutherford Appleton Laboratory, Chilton, Didcot, Oxfordshire OX11 0QX, UK

J. CLAVEL: *IUE* Observatory, ESA, P.O. Box 54065, 28080 Madrid, Spain

A. ELVIUS: Stockholm Observatory, 13300 Saltsjobaden, Sweden

D. PELAT: Observatoire de Paris-Meudon, Place Jules Janssen, 92195 Meudon Principal Cedex, France

M. H. ULRICH: European Southern Observatory, 8046 Garching bei München, Federal Republic of Germany